UNIVERSITÀ DEGLI STUDI DI PAVIA

DIPARTIMENTO DI FISICA

Corso di Laurea Magistrale in Fisica

Radiation protection calculations for an AB-BNCT facility: simulations of patient and treatment room activation

MSc thesis by:
Giovanni Garini

Supervisor:
Prof. Silva Bortolussi
Co-supervisors:
Dr. Chiara Magni

A.A. 2023-2024

Abstract

Un nuovo centro di ricerca e applicazione clinica di *Boron Neutron Capture Therapy* con fascio neutronico prodotto da acceleratore (AB-BNCT) verrà costruito a Caserta nell'ambito del progetto PNC-PNRR ANTHEM. Una facility di BNCT contiene un fascio di neutroni ad alta intensità, per questo motivo gli aspetti legati alla radioprotezione sono di primaria importanza sia nella fase di progettazione che nella gestione del centro. Per ottenere le autorizzazioni per la costruzione e l'utilizzo del centro, deve essere prodotta una relazione con le informazioni rilevanti riguardanti la radioprotezione. Questa tesi descrive il calcolo Monte Carlo di alcuni degli aspetti legati alla radioprotezione che devono essere inclusi nella valutazione complessiva, concentrandosi su quantità dosimetriche e attivazione neutronica. La sorgente neutronica impiegata è quella ottenuta tramite l'acceleratore quadrupolo a radiofrequenza da 5 MeV e 30 mA, accoppiato con un bersaglio di berillio e un Beam Shaping Assmbly (BSA). Queste tecnologie sono in fase di costruzione presso l'Istituto Nazionale di Fisica Nucleare (INFN), ai Laboratori Nazionali di Legnaro e presso la Sezione di Pavia. La geometria dell'edificio, i materiali e le schermature sono stati definiti in lavori precedenti; questa tesi ha sfruttato queste conoscenze per approfondire gli argomenti menzionati sopra. I codici PHITS e D-CHAIN sono stati impiegati per analizzare l'attivazione indotta nei materiali della sala di trattamento dopo lo spegnimento del fascio e per calcolare l'equivalente di dose ambientale prodotta da tale attivazione. I risultati sono utili per valutare l'impatto di questa sorgente radioattiva sia per i pazienti che per il personale del centro. Uno degli elementi più importanti della facility, per quanto riguarda l'attivazione indotta, che è stata qui calcolata, è il BSA. In particolare, è stato valutato l'impatto, sia per il paziente che per il personale, della dose aggiuntiva dopo lo spegnimento del fascio, e sono state proposte contromisure. Anche le apparecchiature nella sala sono una possibile fonte di dose aggiuntiva dovuta all'attivazione, come ad esempio il braccio robotico per il posizionamento dei pazienti, che è stato anch'esso studiato. Un altro aspetto riguarda l'attivazione dei pazienti, che è stata calcolata utilizzando il modello computazionale fornito dall'ICRP, posizionato nella sala di trattamento. Sono state simulate tre posizioni di irraggiamento, che imitano il trattamento di tumori localizzati nel distretto testa-collo, nel torace e negli arti inferiori. Poiché la BNCT è una terapia nuova in ambito clinico, non esistono indicazioni sulla gestione dei pazienti irraggiati. Questa tesi propone un possibile criterio per valutare l'impatto dell'attivazione dei pazienti, rispetto ad altri trattamenti clinici con radiazioni. Si è inoltre studiata l'attivazione delle escrezioni, per stabilire l'eventuale necessità di un bagno "caldo" nella struttura. I risultati di questa tesi saranno soggetti a ulteriori modifiche durante la finalizzazione del progetto dell'impianto, che comporterà ad esempio piccoli cambiamenti nei materiali che compongono il BSA. Tuttavia, gli strumenti computazionali, le metodologie e i criteri di valutazione presentati qui rappresentano un insieme di risorse che contribuiranno in modo significativo al rapporto finale per l'autorizzazione del centro BNCT ANTHEM a Caserta.

Abstract

A new facility for research and clinical application of *Boron Neutron Capture Therapy* with acceleration technology (AB-BNCT) will be built in Caserta (Italy) as part of the PNC-PNRR ANTHEM project. A BNCT facility comprises a neutron beam of high intensity, thus the radiation protection aspects are of primary importance in the design phase as well as in the management of the centre. To obtain the authorizations for the construction and use of the centre a report with the relevant radiation protection information must be produced. This thesis describes Monte Carlo calculation of some of the radiation protection aspects that must be included in the overall evaluation, focusing on dosimetric quantities and neutron activation. The neutron source employed is the one obtained by the 5 MeV, 30 mA radiofrequency quadrupole accelerator, coupled with a beryllium target and a beam shaping assembly. These technologies are being constructed at the National Institute of Nuclear Physics (INFN), National Laboratories of Legnaro and Unit of Pavia. The building geometry, materials and shielding were defined in previous work, this thesis started from this knowledge to assess the mentioned topics. The codes PHITS and D-CHAIN were employed to analyze the induced activation in the materials of the irradiation room after the beam shutdown and to calculate the equivalent ambient dose rate produced by this activation. The results are useful to evaluate the impact of this radiation source for the patients and the centre staff. One of the most important elements of the facility, regarding induced activation is the Beam Shaping Assembly, that was here calculated. In particular, the impact for the patient and staff of the additional dose after the beam shut down was evaluated, and counter measures were proposed. Also the equipment in the room is a source of possible additional dose due to activation, as for example the robotic arm for patient positioning which was tested as well. Another aspect is the patients' activation, that was calculated using the computational phantom provided by ICRP, positioned in the computational reconstruction of the treatment room. Three irradiation positions were simulated, mimicking treatment of tumors located in the head and neck, thoracic and lower limbs districts. As BNCT is a new therapy in the clinical settings, there are no indications on the management of irradiated patients. This thesis proposes a possible criterion to evaluate the impact of the patients activation, compared to other clinical treatments involving radiation. In addition, a focus was dedicated to the excretions activation, to explore the possible need of a hot restroom in the structure. The results of this thesis are subject to further modifications during the finalization of the facility design, which will involve minor changes in the materials of the Beam Shaping Assembly, for example. Nevertheless, the computational tools, methodologies, and evaluation criteria presented here represent a valuable set of resources that will significantly contribute to the final report for the authorization of the ANTHEM BNCT center in Caserta.

Contents

Chapter 1

Introduction

Boron Neutron Capture Therapy (BNCT) is a form of hadrontherapy based on the $^{10}\mathrm{B}(n,\alpha)^{7}\mathrm{Li}$ reaction started by thermal neutrons impinging on ^{10}B.
The core concept of BNCT is to use boron compounds able to convey higher concentrations of ^{10}B in tumor tissues with respect to healthy ones. Thanks to the high Linear Energy Transfer (LET) and the short range in tissue (5-9 μm) of the neutron capture reaction products, α particles and ^{7}Li ions, it is thus possible to administer a higher dose to the tumor while sparing the normal tissues [1].
The selectivity and the consequent success of the therapy depend on different parameters. The first element is the capacity of the boron compound to preferentially target tumor cells. To date, the formulations that have been used in clinical trials are the sodium borocaptate (BSH) and the Boronphenylalanine (BPA). The latter is the one used in current clinical applications of BNCT and permits to achieve a tumor-to-normal tissue concentration ratio of 3.5 to 1 on average [2]. Recently, a formulation of BPA has become an authorized drug in Japan and it is being used for the BNCT of head and neck and brain tumors [3, 4].
Other important aspects to be taken into account are the ones relative to the beam characteristics. To treat deep-seated tumors, the neutron spectrum should be peaked between 1 and 10 keV to allow for a better penetration in tissues. In fact, the cross section of neutron capture is maximum in the thermal energy range (below 0.5 eV), being equal to 3738 b at 0.025 eV. Epithermal neutrons thermalize in the first layers of tissues and reach the tumor at the most suitable energy to maximise the nuclear reaction in boron. Regarding the neutron flux, according to IAEA recommendations, it should be higher than $1.0 \cdot 10^{9} cm^{-2} s^{-1}$ to allow for the therapeutic dose administration in reasonable irradiation times [5].

The main technologies to obtain a beam with these characteristics are the nuclear reactors or proton accelerators coupled to suitable targets. Reactors produce neutrons via the fission reaction in U-235. Accelerators produce neutrons via nuclear reaction of protons hitting lithium targets, based on the ^{7}Li(p,n)^{7}Be reaction, or beryllium targets, based on the ^{9}Be(p,n)^{9}B reaction [6].
Another relevant parameter is the patient positioning, in particular, the distance of the patient from the beam port must be as shorter as possible to avoid loss of neutron flux due to the scattering in air which changes the beam collimation, increasing the irradiation time and the undesired dose to

the patient [7]. To obtain a beam with a suitable energy spectrum and optimal collimation, a set of moderators and collimators called Beam Shaping Assembly (BSA) is needed [8]. A suitable collimation is needed to reduce both the dose absorbed by the out-of-field healthy organs [8] and the activation induced in the surrounding materials of the room structures, which, in turn, increases the ambient dose. The guidelines published by IAEA recommend a value of the ratio current to epithermal flux not less than 0.7 [5].

The presence of a high neutron flux and the characteristics of the neutron interaction with matter make radiation protection studies a pivotal element in the design of a BNCT facility. In particular, the induced activation is a key factor, constituting a radiation protection issue that drives the selection of materials and the project of the centre itself. When the beam designed is optimized for the treatment, the project of the building and the ancillaries present in the rooms must include materials with low activation cross section and/or short lifetime of the activated nuclei. Moreover, the employ of neutron absorbers in the construction elements can help in controlling activation, as described in [9, 10].

1.1 The ANTHEM project

The project ANTHEM (AdvaNced Technologies for Human-centrEd Medicine) is financed by the National Plan for NRRP Complementary Investments (PNC) in the call for the funding of research initiatives for technologies and innovative trajectories in the health and care sectors. Its purpose is to fill, with the help of multidisciplinary and innovative technologies and paths, the existing gap in the healthcare of fragile and chronic patients within specific territories, characterized by pathologies that lack effective therapies.
The project is organized into four spokes with different aims: Spoke 1 "data and technology driven diagnosis and therapies"; Spoke 2 "Connecting patients and therapists through adaptive environments and intelligent sensors to enhance proximity medicine"; Spoke 3 "Risk factors monitoring, diagnostic tools and therapies in chronic disease"; Spoke 4 "Preclinical and clinical breakthrough theranostic and treatments for cancer".
Each Spoke is made up of pilots, addressing specific objectives. The Pilot 9 of the Spoke 4 concerns the construction of a new facility for BNCT research and clinical application in Caserta, at the University of Campania "Luigi Vanvitelli".

The technology to generate the neutron beam is designed and built by National Institute of Nuclear Physics (INFN) and it is based on a proton accelerator, a Be target and a Beam Shaping Assembly (BSA). The accelerator has been developed by the National Laboratory of Legnaro (LNL) and consists in a Radio Frequency Quadrupole (RFQ) machine delivering a 5 Mev, 30 mA proton beam in continuous wave [11]. The proton beam will hit a Be-V-Cu target, also designed at LNL. Finally, the BSA to tailor the energy spectrum and collimation for patients is being developed in Pavia using an innovative method to select the best configuration of materials and to evaluate the therapeutic potential of the beam [8]. A first version of the BSA is described in the cited article, however, the recent re-design of the target and some construction constraints prompted a revision and a simplification of its structure. The new BSA will deliver a flux of the order of $10^{13} cm^{-2} s^{-1}$, as required by the guidelines, starting from a neutron intensity of $10^{14} s^{-1}$ produced in the target.

The Pilot 4.9 of ANTHEM also addresses the design and construction of the building comprising the spaces for the neutron production technology, one patients' irradiation room, one experimental room, and spaces for patients and medical/research staff as shown in the plan in Fig. 1.1.

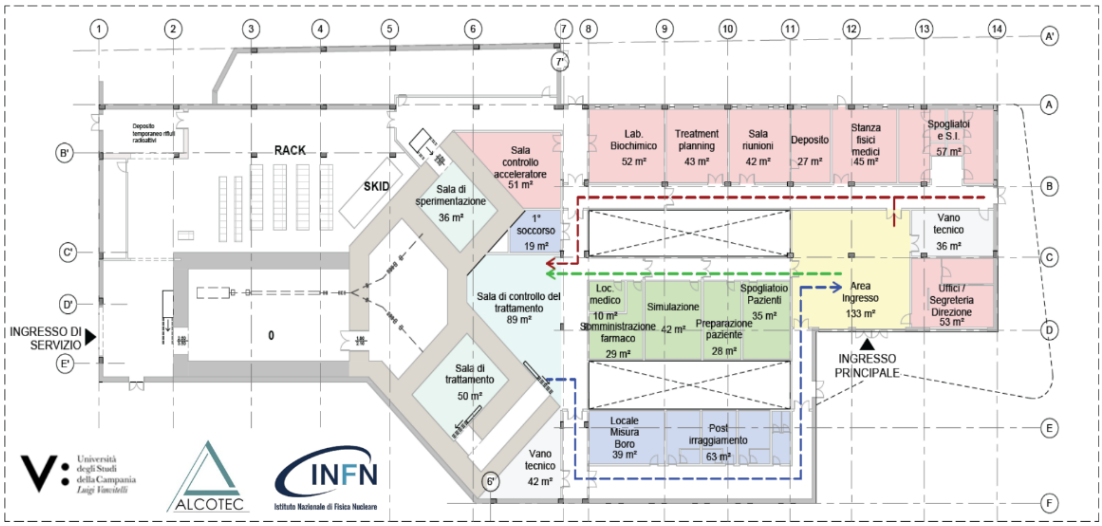

Figure 1.1: Building plan of ANTHEM project facility for BNCT in Caserta.

In the right part of the building plan there are rooms dedicated to the staff and patient preparation, where patients will be received, prepared for boron administration and positioned in a dedicated room matching the irradiation room geometry. Here also laboratories for boron measurements and medical physics will be hosted. Finally, there will be a room for patients' recovery after irradiation. In the central part, the building hosts the irradiation room for the treatment and an additional irradiation room for experimental purposes. In the right-top part of the plan laboratories for radiobiology, biochemistry and molecular medicine will be located. In more details, the personnel rooms from the hospital admission office to the accelerator control room passing through the locker rooms, the rooms for the treatment planning preparation and the biochemical laboratory are marked in pink. The rooms dedicated to the patient pre-treatment phase with the locker room and the rooms assigned at the drug administration are marked in green. The blue areas indicate the post-treatment rooms for the final evaluation of the boron concentration and the controls before the discharge.

The accelerator and the ancillaries for the beam production are detailed in Fig. 1.2.

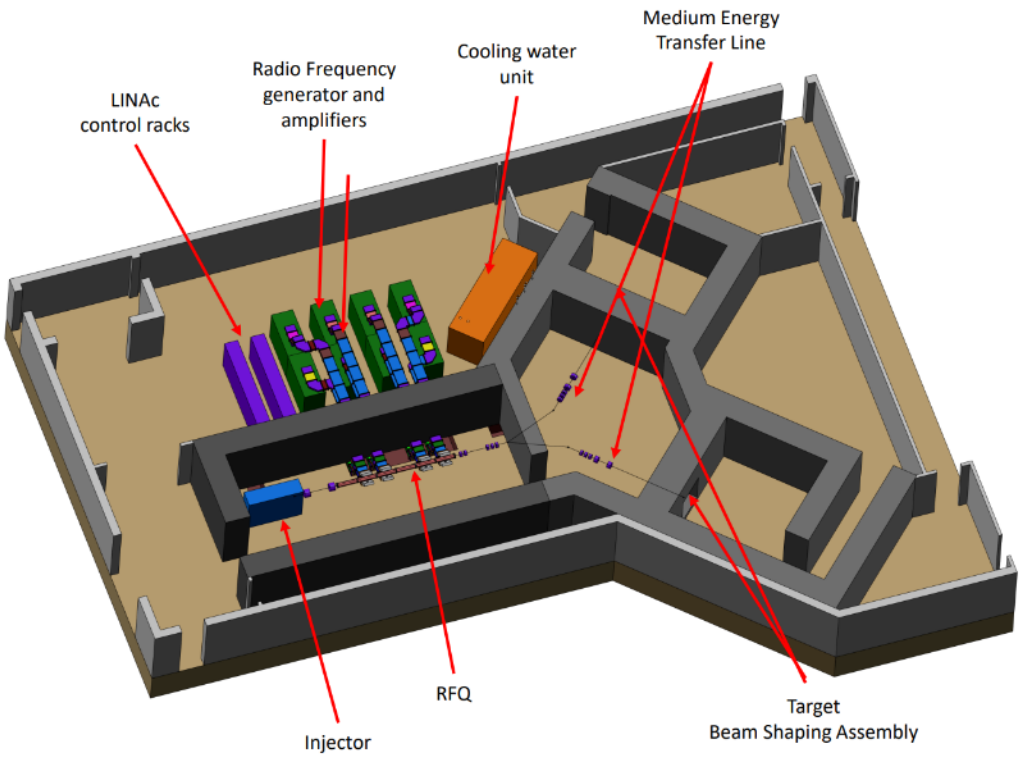

Figure 1.2: The structure of the building showing the areas dedicated to the accelerator and its technical ancillaries and the two irradiation rooms.

1.2 Radiation protection

When there is a need to use radiation, both in industrial or hospital settings, it is necessary to refer to radiation protection principles to protect people from the harmful effects of ionizing radiation. In Italy all the regulations in the field of radiation protection are collected in the legislative decree D. Lgs. 101/2020 which transposes the European Directive 2013/59/Euratom [12].
Among the main radiation protection concepts described in this decree, there are three principles regulating the dose absorbed that must be respected and considered in the following order when working with radiation:

- *justification*, it establishes that the exposure to a radiation must be justified by higher, individual or collective, benefits obtained, compared to the negative effects statistically predictable;
- *optimization*, it is summed up in the *ALARA* principle for which the population exposure to radiation must be kept *As Low As Reasonable Achievable* in relation with the economic and social environment;
- *dose limits*, under which the individual dose must be kept, even when the two previous principles are satisfied.

In the decree, some operational quantities are also defined, which are used in practical applications involving external exposure. The most used to evaluate the dose in air is the ambient equivalent dose H*(d) which is "the dose equivalent at a point in a radiation field that would be produced by the corresponding expanded and aligned field in the ICRU sphere at a depth "d" on the radius vector opposing the direction of the aligned field", in the SI it is measured in Sievert (Sv) [13].
In this definition:

- "d" is measured in millimeters and it can be chosen among 0.7mm, 3mm and 10mm according to the used radiation type, from the less penetrating to the more penetrating one;
- "aligned and expanded field" is a field with uniform fluence and energy distribution and the former is unidirectional [13];
- "ICRU sphere" is a 30 cm sphere with a density of 1 $\frac{g}{cm^3}$ and it is composed by 76.2% oxygen, 11% carbon, 10.1% hydrogen and 2.6% nitrogen (all the percentage to be intended as mass percentage).

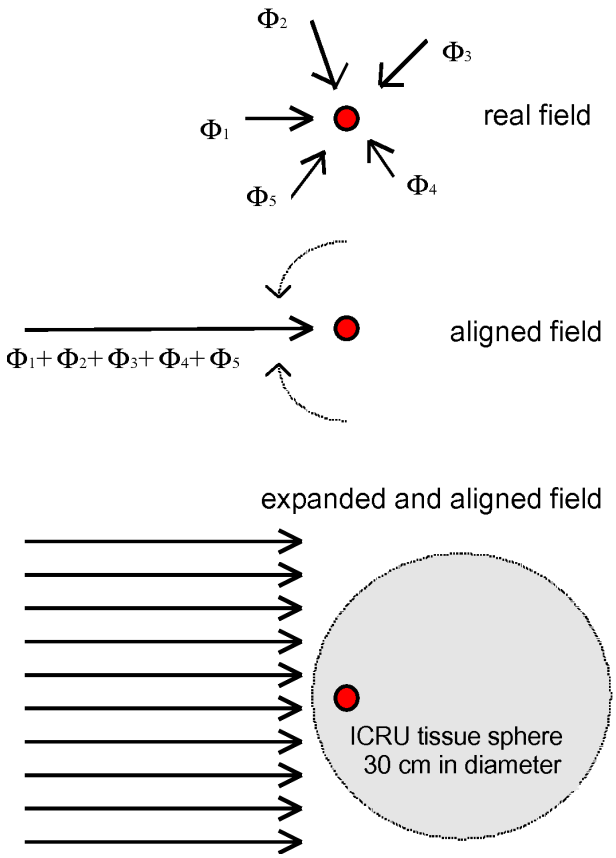

Figure 1.3: Aligned and expanded field definition. Image taken from [14].

Recently in report ICRU 95 [15] it has been introduced a new quantity H*, called ambient dose.

This new quantity is defined as the product between the particle fluence in a point and a conversion coefficient, h* , that relate the particle fluence to the maximum value of the effective dose.

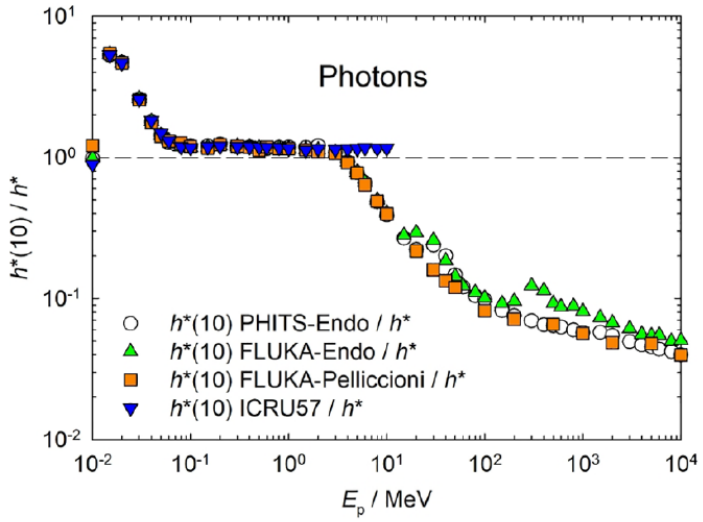

Figure 1.4: Comparison between H*10 and H* conversion coefficients. Taken from [16].

Figure 1.4 from ICRU95 shows the ratio of the conversion factors for the ambient dose equivalent (H*10) and for the ambient dose (H*). As a consequence of this figure, as it is also described in [17], for the purpose of this work H* is well represented by the calculation of H*(10) which is more straightforward because the coefficients are already embedded into the typical Monte Carlo transport codes.

The use of high-intensity neutron beams in BNCT makes the dose calculation more complex compared to the others type of radiation therapies. Due to their nature, neutrons release their energy in matter through nuclear interactions. One of the main issues is the neutron activation of the materials in the room which is due to reactions occurring when an atomic nucleus captures a neutron, the resulting nucleus is in an excited state and can decay in different ways as the following:

- *alpha*, the nucleus decays with emission of an alpha particle, $^4_2$He, with high LET and short range (5-11 cm in air) [18];
- *beta*, it can be β^+ or β^-, in the first one a proton converts in a neutron emitting a neutrino and a positron, in the second a neutron converts to a proton emitting an antineutrino and an electron. Positrons and electrons are called β particles and have higher range with respect to α particles;
- *gamma*, is the production of a photon due to the decay of the excited nucleus. It is the most penetrating radiation.

The behavior of neutron capture cross section generally is described by a 1/v law so it is higher

at lower energy. Due to the use of low energy neutrons in BNCT, neutron activation is thus not negligible. In the design and commissioning of a new facility it is important to calculate the expected activation and to reduce it as much as possible. The activation of materials, like air or walls, can be in fact a problem for patients, for the hospital staff and for the machine technicians, especially when the consequence is a γ decay, characterized by a long range. It can be also a problem for the future decommissioning of the structure, especially when the induced radioisotopes have long half-lives. With the same principle, neutrons can generate activation in the patients and in their excretes, which can influence the post-irradiation management of patients and the design of the centre itself (i.e., construction of dedicated rooms to host patients after the treatment and dedicated restrooms).

This work is devoted to the calculations and the evaluations of neutron activation in the patient body and in some structures of the irradiation facility. The results help predicting the ambient dose produced by the induced radioactivity and give some important indications for the management of the center and the patients from the radiation protection point of view.

Some examples of neutron activation reactions in different materials typically present in a BNCT facility and producing radioactive isotopes are:

- $^{40}\mathrm{Ar}(n,\gamma)^{41}\mathrm{Ar}$ which is present in air;
- $^{23}\mathrm{Na}(n,\gamma)^{24}\mathrm{Na}$, in human body ;
- $^{27}\mathrm{Al}(n,\gamma)^{28}\mathrm{Al}$, in concrete and in BSA.

The radiation protection rules are different for the patient and the medical staff according to the three principles mentioned before. For the former, the extra-dose due to the activation of the elements in the human body is justified by the benefits of the therapy. However, activation of patients must certainly be studied and characterized for the management of the post-irradiation phase. Patients activation can in fact be a problem for people who will come into contact with them after the treatment, such as medical staff and family members. For this reason, it is necessary to evaluate the patient induced radioactivity and to calculate the dose that a person will absorb by being in proximity of the patient. This is one of the calculations performed in this work. Because there are no indications about BNCT, this thesis proposes a possible criterion to evaluate the relevance of the activation of patients irradiated with neutrons. Annex XXV of D.Lgs. 101/2020 establishes a rule in case of nuclear medicine, where patients are administered radioactive drugs. The patient can be discharged without the need for hospitalization for treatments with Iodine-131 administered in activities lower than 600 MBq. In this work, I compared the dosimetry due to the activation of a patient treated with BNCT to that of a patient treated with 600 MBq of Iodine-131. The different situations would require a deeper analysis to ensure that this indicator is a valid benchmark to take operative decisions, however it represents a starting point to understand the magnitude of the effect, using a reasonable comparison approach.

An issue related to the activation of elements in patients is the excretion. One example is the urine, which activates during irradiation. The approach to manage this problem is to build dedicated restrooms which collect the excretions in special shielded tanks, called delay tanks, for the time needed for the activity to decrease below the limits. Then the content can be eventually be released in the sewerage system [19].

Another point addressed in this thesis, is the dose absorbed by patients and eventually by medical staff due to the activation of the materials in the irradiation room. After the shutdown of the beam, the patient needs to stay in the room for a short period of time, during which the radioactivity in the room decreases below a certain threshold for the entrance of the medical staff. In this situation, it is important to lower the extra-dose absorbed by patient due to the activation of the materials: air, walls and equipment. In particular, it is necessary to avoid the dose from BSA activation (the part of the facility which is exposed to the highest neutron fluence), by moving the patient away from the beam-port and/or shielding the beam-port itself with a shutter [10]. For the workers professionally exposed to radiation, dose must remain below the limits set by the decree which are 20 mSv/year of effective dose, 20 mSv/year of equivalent dose to the crystalline lens and 500 mSv/year of equivalent dose to the body extremities or skin, averaged over 1 cm^2 regardless of the exposed surface area [20]. For operative purposes it is useful to evaluate the H*(10) to estimate the risk for the staff working in a controlled area, being H*(10) the main operational quantity for area monitoring.

To overcome the complexity of dose calculation especially when neutrons are involved, the typical approach is the use of Monte Carlo (MC) transport codes which permits to obtain information, like flux, current and dose, through the simulation of radiation transport and interactions. This approach works using a series of functions which describe the occurring interactions called probability density functions (PDFs) that must be non negative, real valued and their integral over their range must be 1. Once a PDF has been defined, using algorithm generating pseudo random numbers, it is possible to sample random values from this function. One of the most used sampling method is the inversion one, here I report an example considering the exponential distribution used to sample the distance of the next interaction for photons [21].

The PDF in this case is:

$$f(x;\lambda) = \lambda e^{\lambda x} \tag{1.1}$$

where λ is the mean free path that is the mean travel of a photon between two interactions. When this method is used it is necessary to obtain the cumulative density function (CDF) which is the integral of the PDF between 0 and x. For the exponential function is:

$$F(\lambda;x) = 1 - e^{-\lambda x}. \tag{1.2}$$

It is now possible to sample a number $\mu \in [0,1)$, locate that on the x-axis of the CDF and calculate:

$$x = F^{-1}(\mu) \rightarrow x = -\frac{ln(1-\mu)}{\lambda}. \tag{1.3}$$

In this way it is possible to sample random numbers from any PDF and, repeating this process for each interaction, the simulation of the transport of radiation in matter is carried out. The quantity we are interested in, called *tally*, is calculated averaging the contributions of each transported particle in the scoring position. For this reason, to obtain a statistically valid result, it is important to repeat the described simulation for a large number of single particles to reduce the relative error.

1.3 PHITS and MCNP

Among the most used MC transport codes when dealing with neutrons there are PHITS (Particles and Heavy Ions Transport code System) [22] and MCNP (Monte Carlo N-Particle) [23]. This two codes are, to some extent, similar: they are both written in Fortran and have similar syntax for the geometry and source definition. To build the geometry of the problem it is firstly necessary to define surfaces that make up the problem and can be infinite planes of different forms or three-dimensional solid surfaces (macrobodies). Then cells are defined using Boolean operations as intersection or union of spaces delimited by the surfaces. The source of radiation is then defined by specifying the type of particles, the geometry of the emitting volume (or surface), the flight direction distribution and the energy spectrum.

PHITS has been developed by JAEA (Japan Atomic Energy Agency) and other institutions, MCNP has been developed by Los Alamos National Laboratory. The main difference between the two codes concerns the data library containing the nuclear data to transport radiation: PHITS uses JENDL-5 [24] instead MCNP uses the Evaluated Nuclear Data File (ENDF) [23]. This difference can produce different results even if the geometry and the sources are defined in the same way.

One of the advantages of PHITS over MCNP is the incorporation of the code DCHAIN-SP, useful for the neutron activation analysis. It is used defining a tally `[t-dchain]` in the PHITS input file setting the parameters of the regions for which induced activity is requested, i.e., how long the source is on and its intensity, then various time output, relative to the moment in which the results are needed (for example, how much time must elapse between the shutdown of the beam and the evaluation of the activation). Running the input file will produce output files called `t-dchain.*` and, running `tdchain.out` with DCHAIN, will deliver some `out-*` files. containing information about the activated isotopes in the selected regions and their activity. There is also a file called `out-phits` that contains the definition of a source with the spectrum of the isotopes activated in the selected regions, that can be used as the source for a new PHITS simulation. This tool is the main reason for choosing PHITS for the simulations in this thesis, however it has been useful to perform a comparison between the flux and the dose values H*(10), due to a 600 MBq ^{131}I source in the thyroid, obtained with the two codes. This is because MCNP has been considered the gold standard for dose calculations in BNCT since many years.

The first step of the simulation concerned the implementation of a phantom representing a patient. Among the most detailed phantoms there were two possibilities: the adult mesh-type computational phantom from the ICRP publication 145 [25] and the voxel-type phantom from ICRP publication 110 [26]. I have chosen the former because it is newer and it is made with a tetrahedral mesh which increases the resolution, especially for small structures, compared to the latter that is made up of a voxel mesh composed by cubes that prevents a smooth definition of objects. This geometry complexity increases the calculation time and PHITS is able to manage it better respect to MCNP so this is another reason to prefer it. The machine used for calculations has two CPU (Intel(R) Xeon(R) CPU E5-2680 v3 @ 2.50GHz) each one with 24 threads and 64 Gb of RAM. To display the geometry PHITS needs few minutes, while MCNP needs some days. This is very unpractical because geometry visualization is typically needed for debugging. Due to the particular type of mesh implemented in MCNP, the parallel calculation is not possible. This is

another disadvantage as the computing time for simulation thus diverges. PHITS, on the other hand, can implement parallel calculation, obtained by inserting `\$OMP= number of threads` at the beginning of the input file.

The tetrahedral phantom is downloaded in a folder containing an example of implementation both for MCNP and PHITS, and four files for each phantom `MRCP-AM.*` (male model) and `MRCP-AF.*` (female model).

The files are different for the two codes, for MCNP we find:

- `*.cell` containing the definition of the cells ;
- `*.materials` containing the definition of all materials;
- `*.tally` containing the definition of a tally for each region;
- `*.inp`, an example of this file is reported below, focusing on the region 13200 which represents the thyroid. It contains the definitions of regions, called `Part`, composed by tetrahedrons. For each Part we have than the position in space of the `nodes` of the tetrahedrons, the definition of each tetrahedron (`element`) through the choice of four nodes and the recall of a material defined in the other file.

```
*Part, name=Part-132000000
*Node
+--2408 lines: 1,  -0.1576530000, -0.6386820000,
56.3224950000----------------------
*Element, type=C3D4
+--8687 lines: 1,  1,  2,  3,  4----------------
*Nset, nset=Set-material_13200, generate
1,   2408,   1
*Elset, elset=Set-material_13200, generate
1,   8687,   1
*Nset, nset=Set-statistic_13200, generate
1,   2408,   1
*Elset, elset=Set-statistic_13200, generate
1,   8687,   1
*Elset, elset=Set-source_13200, generate
1,   8687,   1
*End Part
```

In this case, to set the ^{131}I source in the thyroid it is necessary to modify the `MRCP-*.inp` file by inserting in the definition of the `Part 13200` (the thyroid):

```
Elset, elset=Set-source_13200, generate 1. 8687, 1
```

and defining the source in the main MCNP file as follows:

```
SDEF par=p erg=D1       $ General source definition
pos=volumer             $ Recall the source definition in the .inp file
SI1 L 0.284 0.365 0.637 $ energy probability
SP1 D 0.061 0.817 0.072 $ emission energies
```

.

The file in the folder for PHITS simulations are:

- `*.node` with the definition of the nodes;
- `*.element` with the definition of the tetrahedrons and the assignation of a universe number;
- `*.material` with the materials definition;
- `*.cell` in which are defined all the cells composed by the universes defined in the `*.element` file.

In this case the source definition in the PHITS input file is:

```
    [ S o u r c e ]
   s-type =   24
   tetreg = 13200
     proj =  photon          # kind of incident particle
      dir =   all            # z-direction of beam [cosine]
   e-type =   8              # Discrete source definition
       ne =   3              # number of discrete values
#      e(i)    w(i)
     0.365     0.817
     0.637     0.072
     0.284     0.061
```

describing, respectively, the position, the type of particle, the flight direction and the energy spectrum.

After defining the source, the goal was to calculate the photon flux for a comparison. I have thus requested a tally in a cylindrical mesh, with axis along the vertical axis of the phantom, coinciding with the z direction. I have tallied the upper part of the phantom from z=0 to z=80 cm and radially from r=0 to r=120 cm both in steps of 10 cm. The tally in MCNP was defined as follows:

```
FMESH4:p geom=RZT origin= 0.0, 0.0, 0.0
         imesh=120  iints=12
         jmesh=80.0 jints=8
         kmesh=1    kints=1
```

and for PHITS it was:

```
[ T - T r a c k ]
  title   = flux (1/cm^2/source)
   file   = flux.out
   mesh   = r-z
       x0 = 0.0
       y0 = 0.0
  r-type  =  2
     nr   =  12
     rmin =  0.0
     rmax = 120.0
  z-type  =  2
```

```
    nz    =   8
    zmin  =   0
    zmax  =  80
    part  = photon
  e-type  =    1
     ne   =    1
              0.0   1.0E+03
    unit   =    1
    axis   =    r
   gshow   =    1
   epsout  =    1
   z-txt   =    Flux [1/cm^2/source]
```

In both outputs, the result obtained is given in $cm^{-2} \cdot source^{-1}$: the flux in $cm^{-2} \cdot s^{-1}$ due to 600 MBq of ^{131}I concentrated in the thyroid is obtained by multiplying for the source activity in Bq because for each decay there is only one photon emitted.

As a figure of merit to evaluate the difference between the two codes, I have chosen MCNP as the truth and I have calculated the relative difference (RD) as:

$$RD = \frac{|\phi_{MNCP} - \phi_{PHITS}|}{\phi_{MNCP}}. \tag{1.4}$$

For each zone of the mesh RD is below 9% and in 68.5% of the results RD is below 5%. Table 1.1 also reports the comparison of the total flux in the cylinder for the two codes.

MCNP ($cm^{-2} \cdot s^{-1}$)	PHITS ($cm^{-2} \cdot s^{-1}$)	Percentage variation (%)
$5.20{\cdot}10^{6} \pm 3.17{\cdot}10^{3}$	$5.56{\cdot}10^{6} \pm 2.42{\cdot}10^{4}$	6.9

Table 1.1: Comparison of MCNP and PHITS flux calculations

To obtain a comparison in terms of dose H*(10) the simulations were repeated in the same conditions adding multiplicative factors to convert flux in ambient equivalent dose. H*(10), in fact, can be calculated from the flux using tabulated multiplying factors depending on the type of the particle and on its energy and are obtained with detailed simulations and calculations. These tables are given by ICRP (International Commission on Radiation Protection) and ICRU (International Commission on Radiation Units and measurements), entities that have been created with the task of define, respectively, the recommendations and the units to be adopted in contexts where radiation protection is necessary.

To add a multiplier to MCNP tally, two sets of values are provided: `DE\#` and `DF\#` where # is the number of the tally in use (in this case it is tally-type 4, that calculates flux using track-length estimator, see [23]). These factors works linking a factor in the DF column to an energy interval in the DE column, so the dose due to a photon in a certain energy bin is obtained multiplying the flux (calculated by MCNP in that energy bin) by the relative factor. The factors for the energies missing in DE, as the one between two values, are automatically obtained interpolating the factors with a logarithmic function.

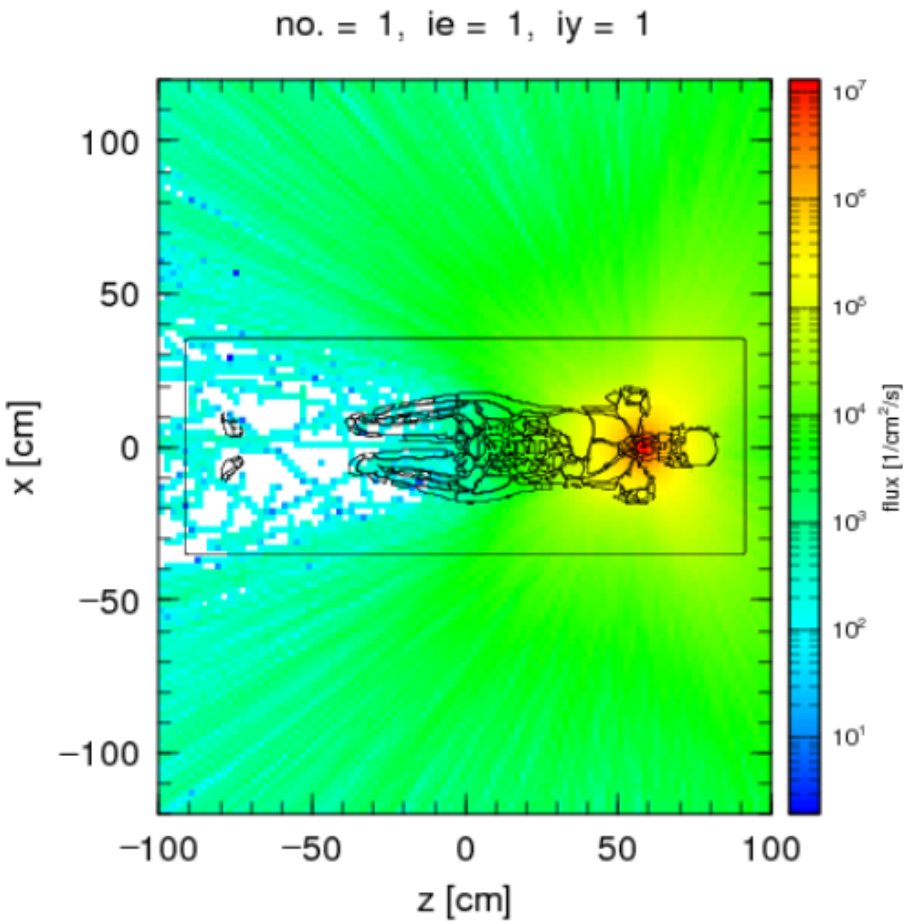

Figure 1.5: Flux in a radius of 1.2 m around the patient due to 600 MBq of ^{131}I in the thyroid.

The conversion factor tables used in this evaluation come from [16] which is the latest release by ICRU and ICRP reports.

In PHITS it is possible to use multipliers directly in a tally inserting the following lines:

```
multiplier = 1
mat    mset1
1    (1.0 -251)
```

defining the number of the material for which H*(10) must be calculated (`1` in this case, corresponding to air) and the number indicating the multiplier. PHITS permits both to define new multipliers in a [Multiplier] section or use default multipliers (-200 is used to calculate H*(10)). To obtain a consistent comparison, I used the same factors for the two codes thus I defined the multiplier `-251` and asked PHITS to interpolate with a logarithmic function to match the MCNP calculation.

After these simulations I evaluated the dose difference in percentage, with the same formula used for the flux. For all the mesh regions except one, the values of the relative difference of dose were

below 5%. Table 1.2 reports the dose values obtained in the whole cylinder.

MCNP (pSv $\cdot s^{-1}$)	PHITS (pSv $\cdot s^{-1}$)	Percentage variation (%)
$7.00{\cdot}10^{6} \pm 4.15{\cdot}10^{3}$	$7.16{\cdot}10^{6} \pm 3.19{\cdot}10^{4}$	2.3

Table 1.2: Comparison of MCNP and PHITS H*(10) calculations.

It is interesting to observe that the discrepancy between the dose values is lower than the one obtained in flux calculations. This may be attributed to the logarithmic interpolation which compensates for the flux difference.

Figure 1.6 shows the results of the dose calculation in PHITS with a larger mesh going from z=-80 cm and z=80 cm (whole body height) that was useful to define the limit for the patient discharge. From this point onwards in the thesis, any mention of H*(10) will refer specifically to a dose rate.

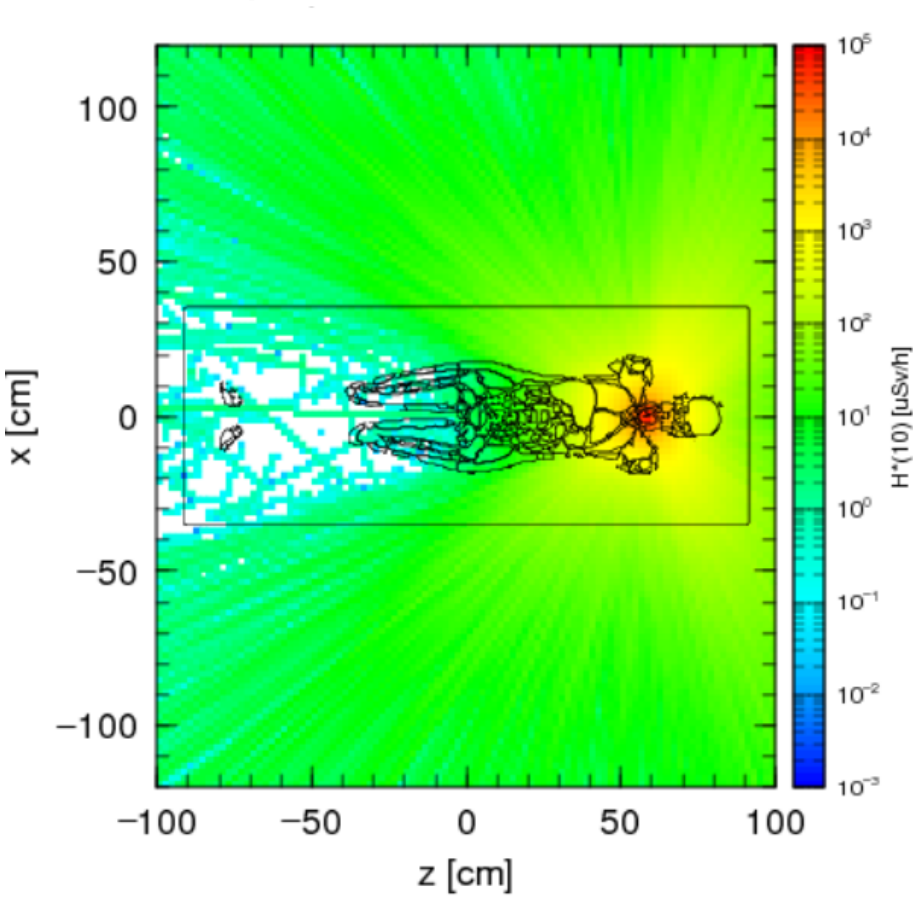

Figure 1.6: H*(10) in a radius of 1.2 m around the patient due to 600 MBq of ^{131}I in the thyroid.

Table 1.3: H*(10) around the patient due to 600 MBq of ^{131}I in the thyroid.

Radius (cm)	H*(10) 1h irr. (μSv/h)	Rel. err.
30-40	$1.15{\cdot}10^{3}$	$7.61{\cdot}10^{-3}$
40-50	$8.18{\cdot}10^{2}$	$8.56{\cdot}10^{-3}$
50-60	$6.22{\cdot}10^{2}$	$9.28{\cdot}10^{-3}$
60-70	$4.94{\cdot}10^{2}$	$9.91{\cdot}10^{-3}$
70-80	$4.05{\cdot}10^{2}$	$1.04{\cdot}10^{-2}$
80-90	$3.40{\cdot}10^{2}$	$1.09{\cdot}10^{-2}$
90-100	$2.89{\cdot}10^{2}$	$1.12{\cdot}10^{-2}$
100-110	$2.49{\cdot}10^{2}$	$1.16{\cdot}10^{-2}$
110-120	$2.17{\cdot}10^{2}$	$1.19{\cdot}10^{-2}$

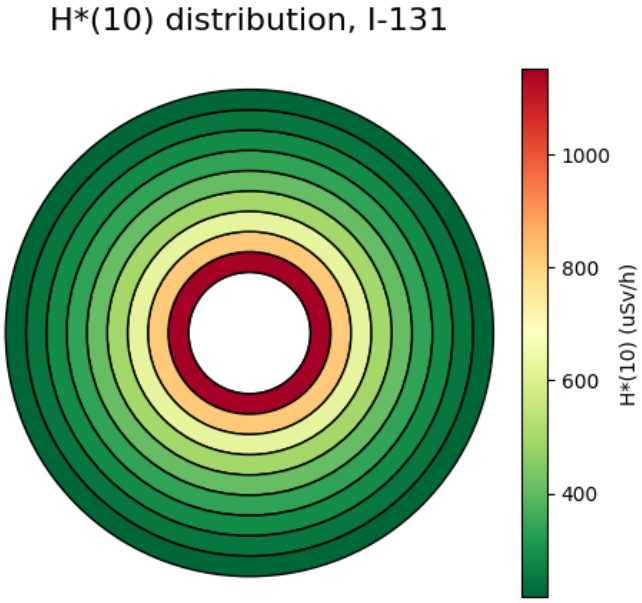

Figure 1.7: Transversal vision map of the values in table 1.3.

Table 1.3 shows the values of H*(10) around the patient from a distance of 30 cm to 120 cm due to an activity of 600 MBq of ^{131}I placed in the thyroid. These values are graphically reported in figure 1.7 which shows a transverse map of the ambient dose around the patient. Both the table and the figure will be useful in the next chapter to make a comparison with the results for the irradiation conditions.

Chapter 2

Patient Activation

As anticipated in the previous Chapter, a reasonable criterion to evaluate the impact of patients' activation after BNCT is to compare the ambient dose after a treatement with the ambient dose generated by a patient who underwent radionuclide metabolic therapy with 600 MBq of iodine-131. According to the decree, in fact, in this case the patient can be discharged without further hospitalization. The idea is that, when the ambient dose distributions are comparable, also the BNCT patient could be discharged, allowing to anticipate the post-irradiation phase in the new center (i.e. how much time the patients must remain in the center).

For this calculation it is essential to reproduce accurately the geometry of the treatment room to consider all the interactions of neutrons that will produce activation in the patient's body. Neutrons in fact can either be absorbed in the patient, or scatter in the room components back to the patient.
Figure 2.1[a] represents the geometry of the whole facility described in the previous Chapter reproduced in PHITS.

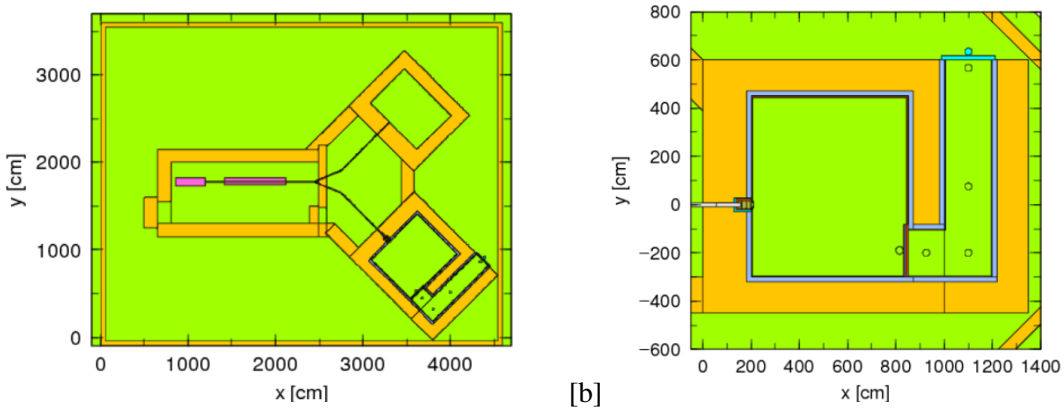

[a] [b]

Figure 2.1: Facility geometry in PHITS [a] and a particular of the treatment room [b].

Figure 2.1[b] shows the treatment room geometry. The neutron source (i.e. the Be target and the BSA) is embedded in the wall on the left wall, ending the beam-port in front of which the patient

must be positioned for the irradiation. On the right of the figure there is a maze used to prevent radiation from escaping the room thanks to the energy loss due to scattering. The maze is closed with two doors made by 15 cm of borated polyethylene and 5 cm of lead for the internal one and 2 cm for the external one.
The internal wall composition of the treatment room has been assessed through the calculation of ambient dose equivalent, due to neutron and photons, in some different scenarios varying the thickness and the materials composing the walls. The results proved that the best solution, in terms of radiation protection and of construction was to use three layers: the external one made of borated polyethylene 5 cm thick layer working as a neutron absorber (30% natural boron), then 20 cm of baritic concrete used as a photon absorber and lastly 1.3 m of Portland concrete.

Once the room geometry was modeled it was necessary to position the patient in front of the beam-port. I have decided to evaluate the patient activation in three different irradiation positions simulating the treatment of cancers located in the head-neck region (Fig.2.2[a]), in the thorax (Fig.2.2[b]) and in the lower limbs (Fig.2.2[c]).

The positions reported in Fig. 2.2 were not optimized for the treatment purpose: they are representative for the study the activation. Each tumor, in fact, requires a precise patient positioning that must be individually considered during the treatment planning to maximize the dose absorbed by the tumor while respecting the dose constraints in the surrounding organs at risk.

For each position I simulated the neutron irradiation. The neutron source, coming from the (p,n) reaction on Be, has been defined using the experimental double differential spectra described in[27]. The source is well validated [8] and the spectrum irradiating the patient is obtained by a preliminary designed version of a BSA.

The number of neutrons for each simulation has been chosen evaluating the uncertainty in each cell composing the phantom when tallying neutron flux, with a `[T-Track]`. In order to avoid an increase of the calculation time, I fixed as an acceptable threshold a relative error lower than 15% in cells where the flux is, at most, two order of magnitude lower than the maximum value. This required to simulate, for each irradiation position, 100 batches of 10^6 neutrons each, to obtain statistically significant results.

To obtain information about patient activation I have used a `[T-Dchain]` tally on each region composing the phantom and considering 1 and 2 hours of irradiation time with two different tallies. For each of these tallies I have used five output times, one at the end of irradiation (0s) and 10, 15, 30, 45 minutes after the beam shutdown. An example of the 1h tally is:

```
[ T - D c h a i n ] $1 h irradiation
$  must section for DCHAIN
     mesh =  reg            $ mesh type is region-wise
     reg =  100 200 300 301 302 303 400 401 402 403 404 405 500 501 600 700 800
     801 802 803 804 805 806 807 808 900 910 1000 1010 1100 1110 1200 1210 1300
     1400 1500 1600 1700 1800 ... 13700 13701 13800 13900 14000
     file =  tdchain2.out        $ file name of dchain-sp input file
     timeevo =    2               $ time evolution
     1.0 h  1.0      $ with 1.0 = irradiation time                          - C
     1.0 h  0.0     $ with 0.0 = cooling time N.B: must contain all OUTTIMES - C
     outtime =   5              $ output time
```

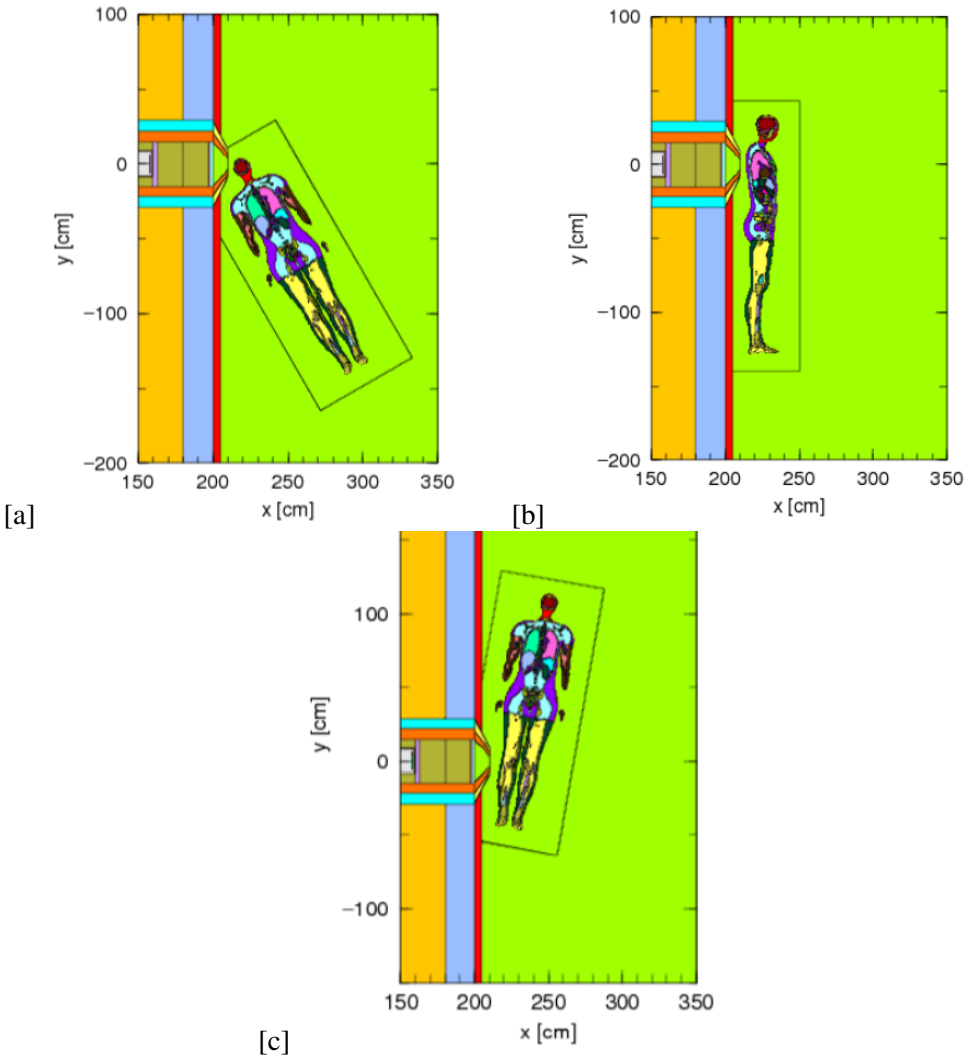

Figure 2.2: Patient irradiation positions for cancers located in: neck-head region [a], thorax [b], lower limbs [c].

```
1.0 h $ end of irradiation
-10 m $ 10 min after irradiation
-15 m $ 15 min after irradiation
-30 m $ 30 min after irradiation
-45 m $ 45 min after irradiation
$ beam current (nA)
amp = 1e14   $ (D=1.0) Source Intensity(source/sec)
```

The outputs of these tallies are then used as an input for DCHAIN, leading to obtain, for each region and output time, information about the activated nuclides, in the `spd-act.out` file, or a file called `out-phits` containing a list of the PHITS sources generated by the region's activation.

These files are useful to identify the most activated regions, the isotopes generated and their half lives. In particular I focused on the dose produced by the activation at 15 minutes after the beam shutdown. This time interval is meaningful because we know from other facilities that are currently treating patients, that the time elapsed between the end of the irradiation and the entrance of the medical staff is of the order of 15 minutes.

To obtain information about the dose due to the patient activation and to make them comparable to the case of ^{131}I, a new input file with the patient in the same condition of the previous calculations was prepared. Tallies were defined as in the Iodine case as well. The generation of a new file was necessary because H*(10) is calculated with multipliers which are valid in air; the patient in the room is surrounded by different materials which would make it impossible to use the multipliers.

Once the new geometry has been changed the sources is defined starting from the `out-phits` given from DCHAIN. This file contains the sources, for each tallied regions, generated by the activation. An example of the `out-phits` file content for region N°100 is:

```
[ S o u r c e ]
 totfact =   3.3944E+02  $ total number of gamma-rays (n/sec/cc) x volume (cc)
  s-type =   5
    proj = photon
     reg =      100 $ This cell ID  should be revised for lattice  or combined cell case
      x0 =          $ Input minimum x of the region here
      x1 =          $ Input maximum x of the region here
      y0 =          $ Input minimum y of the region here
      y1 =          $ Input maximum y of the region here
      z0 =          $ Input minimum z of the region here
      z1 =          $ Input maximum z of the region here
     dir = all
  e-type = 4
      ne =     37
$     Energy  Flux (arbitrary unit)
$             ^^^^ Energy spectra (n/sec/cc) based on activity concentration (Bq/cc)
      0.0010  0.0000E+00
      0.0100  0.0000E+00
      0.0200  0.0000E+00
      0.0300  0.0000E+00
      0.0450  0.0000E+00
      0.0600  0.0000E+00
      0.0700  0.0000E+00
      0.0750  0.0000E+00
      0.1000  5.6293E-21
      0.1500  2.7234E-19
      0.2000  1.4249E-16
      0.3000  1.9123E-03
      0.4000  1.1663E-17
      0.4500  3.9515E+01
      0.5100  1.2844E-06
      0.5120  3.4727E-15
      0.6000  2.2059E-05
      0.7000  0.0000E+00
```

```
 0.8000  3.8778E-04
 1.0000  1.1089E-03
 1.3300  0.0000E+00
 1.3400  2.3376E+00
 1.5000  3.3045E+00
 1.6600  2.7613E-04
 2.0000  3.9487E+00
 2.5000  2.4183E+00
 3.0000  5.9386E-03
 3.5000  4.7446E-03
 4.0000  1.9580E-06
 4.5000  0.0000E+00
 5.0000  9.5456E-17
 5.5000  0.0000E+00
 6.0000  2.7450E-04
 6.5000  1.6267E-07
 7.0000  2.0092E-05
 7.5000  0.0000E+00
 8.0000  3.1293E-07
10.0000
```

For a tetrahedral mesh, to define the source position, it is possible to remove the x,y,z coordinates and change `s-type=5` in `s-type=24` and `reg` in `tetreg`.

In each PHITS source the value of produced particle, gamma in my case, is given by the `totfact`. Generally, to define multiple sources in a single PHITS input it is necessary to set a single `totfact` which is the maximum one between all the sources. Then, for each source, define a `<source>` parameter obtained from the normalization of each source production with respect to the `totfact`. To decrease the calculation time, I defined the sources only in the cells with an activity, at most, two orders of magnitude lower than the highest value.

2.1 Results

To evaluate the activation of the patient I simulated the irradiation for two different times, 1 and 2 hours, the first one being similar to the real BNCT treatment, the second representing a more conservative condition. This section reports, for each irradiation position and irradiation time, the ambient dose equivalent from z=-80 cm to z=80 cm in a radius of 1.2 m, to be compared to ^{131}I described in Chapter 1. In addition, it reports the isotopes with the highest activity and their half lives, which permits to estimate the residual radioactivity after a certain time. It is important to stress that all the activities and total numbers of produced gamma rays that will be reported in this thesis are not strictly correlated with the ambient dose. This quantity in fact not only depends on the gamma flux, but also on photons energy. Anyway the number of the produced photon can be a first indicator of the expected dose.

2.1.1 Irradiation of the head and neck district

When the patient is positioned for irradiation of the region of the head and neck, the three most activated regions are:

- N° 2600, the cranium cortical bone;
- N° 2700, the cranium spongiosa bone;
- N° 6100, the brain.

Figure 2.3 shows the head geometry. In particular region 2600 is represented in light brown, region 2700 in beige and region 6100 in blue.

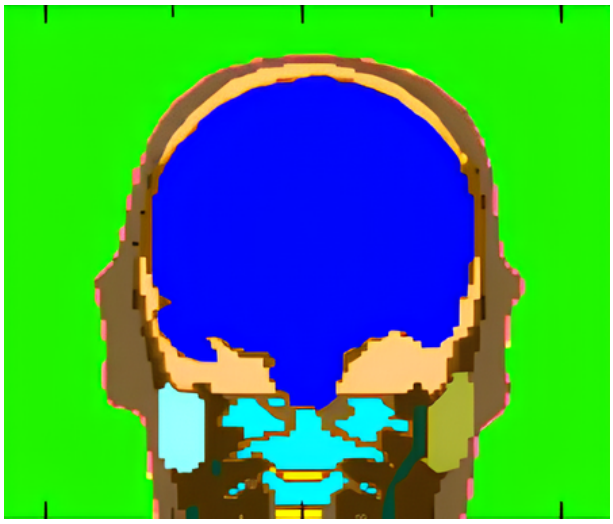

Figure 2.3: Head geometry particular.

This is valid for both the simulated irradiation times. Table 2.1 shows the total number gamma-rays (the `totfact`) for both irradiation times at 15 minutes after the shutdown.

Table 2.1: Total number of γ-rays for both irradiation times at 15 minutes after the shutdown

Region	1h+15m (s^{-1})	Rel. err.	2h+15m (s^{-1})	Rel. err.
6100	$4.35 \cdot 10^6$	1.0%	$7.25 \cdot 10^6$	1.0%
2600	$8.78 \cdot 10^5$	1.0%	$1.43 \cdot 10^6$	1.0%
2700	$6.35 \cdot 10^5$	1.0%	$1.05 \cdot 10^6$	1.0%

It is interesting to observe that this number does not become twice by doubling the irradiation time, that is due to the fact that during the additional irradiation hour part of the activated isotopes decay.

Tables 2.2, 2.3, 2.4, 2.5, 2.6,2.7 list, for the three regions, the three most activated isotopes, for 1 hour of irradiation, at the end of the treatment (+0 s) and 15 minutes after the beam shutdown (+ 15 m). The activity reported in this case is the sum of the contributions from all the decay types (beta and gamma). It is interesting to observe these values to have an idea of the most active isotopes. Anyway, only the gamma emission plays a role in the calculation of ambient dosimetry, because charged radiation is absorbed in patient and do not contribute to dose in air.

Table 2.2: Region 6100, 1 h Irradiation + 0 s, statistical uncertainty below 0.5%

Isotope	Activity(Bq)	Relative activity	Half life (s)
^{24m} Na	$1.982 \cdot 10^{7}$	80.29%	$2.018 \cdot 10^{-2}$
^{38} Cl	$3.401 \cdot 10^{6}$	13.78%	$2.234 \cdot 10^{3}$
^{24} Na	$1.192 \cdot 10^{6}$	4.83%	$5.398 \cdot 10^{4}$

Table 2.3: Region 6100, 1 h Irradiation + 15 m, statistical uncertainty below 0.5%

Isotope	Activity(Bq)	Relative activity	Half life (s)
^{38} Cl	$2.572 \cdot 10^{6}$	64.03%	$2.234 \cdot 10^{3}$
^{24} Na	$1.179 \cdot 10^{6}$	29.34%	$5.398 \cdot 10^{4}$
^{42} K	$2.347 \cdot 10^{5}$	5.84%	$4.450 \cdot 10^{4}$

Table 2.4: Region 2600, 1 h Irradiation + 0 s, statistical uncertainty below 0.5%

Isotope	Activity(Bq)	Relative activity	Half life (s)
^{24m} Na	$4.917 \cdot 10^{6}$	72.44%	$2.018 \cdot 10^{-2}$
^{49} Ca	$1.004 \cdot 10^{6}$	14.79%	$5.231 \cdot 10^{2}$
^{49} Sc	$4.368 \cdot 10^{5}$	6.44%	$3.431 \cdot 10^{3}$

Table 2.5: Region 2600, 1 h Irradiation + 15 m, statistical uncertainty below 0.5%

Isotope	Activity(Bq)	Relative activity	Half life (s)
^{49} Sc	$4.598 \cdot 10^{5}$	39.36%	$3.431 \cdot 10^{3}$
^{49} Ca	$3.046 \cdot 10^{5}$	26.07%	$5.231 \cdot 10^{2}$
^{24} Na	$2.925 \cdot 10^{5}$	25.03%	$5.398 \cdot 10^{4}$

Table 2.6: Region 2700, 1 h Irradiation + 0 s, statistical uncertainty below 0.5%

Isotope	Activity(Bq)	Relative activity	Half life (s)
^{24m} Na	$3.350 \cdot 10^{6}$	75.68%	$2.018 \cdot 10^{-2}$
^{49} Ca	$4.257 \cdot 10^{5}$	9.62%	$5.231 \cdot 10^{2}$
^{24} Na	$2.016 \cdot 10^{5}$	4.55%	$5.398 \cdot 10^{4}$

Table 2.7: Region 2700, 1 h Irradiation + 15 m, statistical uncertainty below 0.5%

Isotope	Activity(Bq)	Relative activity	Half life (s)
^{24} Na	$1.993 \cdot 10^{5}$	27.32%	$5.398 \cdot 10^{4}$
^{49} Sc	$1.950 \cdot 10^{5}$	26.74%	$3.431 \cdot 10^{3}$
^{38} Cl	$1.438 \cdot 10^{5}$	19.72%	$2.234 \cdot 10^{3}$

In the three regions, at the shutdown of the beam the main contribution to the activity comes from ^{24m}Na. It decays in ^{24}Na with a gamma emission with a branching ratio of 99.95% and in ^{24}Mg (stable) trough a β^- decay with a branching ratio of 0.05%. Due to the low half life of this isotope (τ=2.018 $\cdot 10^{-2}$) at 15 minutes after the shutdown its contribution is almost zero. It is also interesting to observe that the longest half lives are of the order of 10^4s (some hours). This means that after one day the activity will be reduced of almost one order of magnitude. The fact that isotopes with a half life in the order of some minutes give high contribution to the total activity, suggests that the total activity will be drastically reduced in some days. However, the residual activation after the discharge of patients is not a concern from the point of view of the dose produced and thus does not limit normal life in contact with other people after treatment.

Tables2.8, 2.9, 2.10, 2.11, 2.12,2.13 list the same results but for 2 hours of irradiation.

Table 2.8: Region 6100, 2 h Irradiation + 0 s, statistical uncertainty below 0.5%

Isotope	Activity(Bq)	Relative activity	Half life (s)
^{24m} Na	$1.981 \cdot 10^7$	72.89%	$2.018 \cdot 10^{-2}$
^{38} Cl	$4.513 \cdot 10^6$	16.60%	$2.234 \cdot 10^3$
^{24} Na	$2.331 \cdot 10^6$	8.57%	$5.398 \cdot 10^4$

Table 2.9: Region 6100, 2 h Irradiation + 15 m, statistical uncertainty below 0.5%

Isotope	Activity(Bq)	Relative activity	Half life (s)
^{38} Cl	$3.414 \cdot 10^6$	54.73%	$2.234 \cdot 10^3$
^{24} Na	$2.304 \cdot 10^6$	36.94%	$5.398 \cdot 10^4$
^{42} K	$4.566 \cdot 10^5$	7.32%	$4.450 \cdot 10^4$

Table 2.10: Region 2600, 2 h Irradiation + 0 s, statistical uncertainty below 0.5%

Isotope	Activity(Bq)	Relative activity	Half life (s)
^{24m} Na	$4.917 \cdot 10^6$	65.77%	$2.018 \cdot 10^{-2}$
^{49} Ca	$1.012 \cdot 10^6$	31.79%	$5.231 \cdot 10^2$
^{49} Sc	$7.336 \cdot 10^5$	9.81%	$3.431 \cdot 10^3$

Table 2.11: Region 2600, 2 h Irradiation + 15 m, statistical uncertainty below 0.5%

Isotope	Activity(Bq)	Relative activity	Half life (s)
^{49} Sc	$7.082 \cdot 10^5$	39.37%	$3.431 \cdot 10^3$
^{49} Ca	$5.717 \cdot 10^5$	31.79%	$5.231 \cdot 10^2$
^{24} Na	$3.072 \cdot 10^5$	17.08%	$5.398 \cdot 10^4$

Table 2.12: Region 2700, 2 h Irradiation + 0s, statistical uncertainty below 0.5%

Isotope	Activity(Bq)	Relative activity	Half life (s)
^{24m} Na	$3.350 \cdot 10^{6}$	68.84%	$2.018 \cdot 10^{-2}$
^{49} Ca	$1.374 \cdot 10^{6}$	8.82%	$5.231 \cdot 10^{2}$
^{24} Na	$1.261 \cdot 10^{6}$	8.10%	$5.398 \cdot 10^{4}$

Table 2.13: Region 2700, 2 h Irradiation + 15 m, statistical uncertainty below 0.5%

Isotope	Activity(Bq)	Relative activity	Half life (s)
^{24} Na	$3.895 \cdot 10^{5}$	34.52%	$5.398 \cdot 10^{4}$
^{49} Sc	$3.003 \cdot 10^{5}$	26.61%	$3.431 \cdot 10^{3}$
^{38} Cl	$1.909 \cdot 10^{5}$	16.91%	$2.234 \cdot 10^{3}$

The comparison of these values (2 hours of irradiation) and the previous ones (1 hour) shows that the activity of the ^{24m}Na is the same at the shutdown of the beam. This effect comes from reaching a kind of secular equilibrium at which the production rate of the isotope due to the irradiation is almost equal to its decay rate. Other isotopes have a higher activity, less than twice than for 1 hour irradiation, due to the relatively low half lives which make the element decay during the additional irradiation hour.

Figure 2.4 represents the map of H*(10) for 1 and 2 hours of irradiation at 15 minutes after the shutdown. It is observable that the dose is higher near the head, as expected because the most activated regions are those directly irradiated by the neutron beam.

It is important to highlight that, in correspondence of the patient, the values represented in these images are not correct. This is because H*(10) is calculated multiplying the flux with multiplication factors which must be referred to air only. This is not a concern because the focus is on the dose surrounding the patient and not the dose in the organs, which must be calculated by treatment planning.

Table 2.14 reports the H*(10) results for both the irradiation times at 15 minutes after the beam shutdown. These values are obtained summing up H*(10) over the whole height of the mesh for each annulus of the cylindrical mesh.

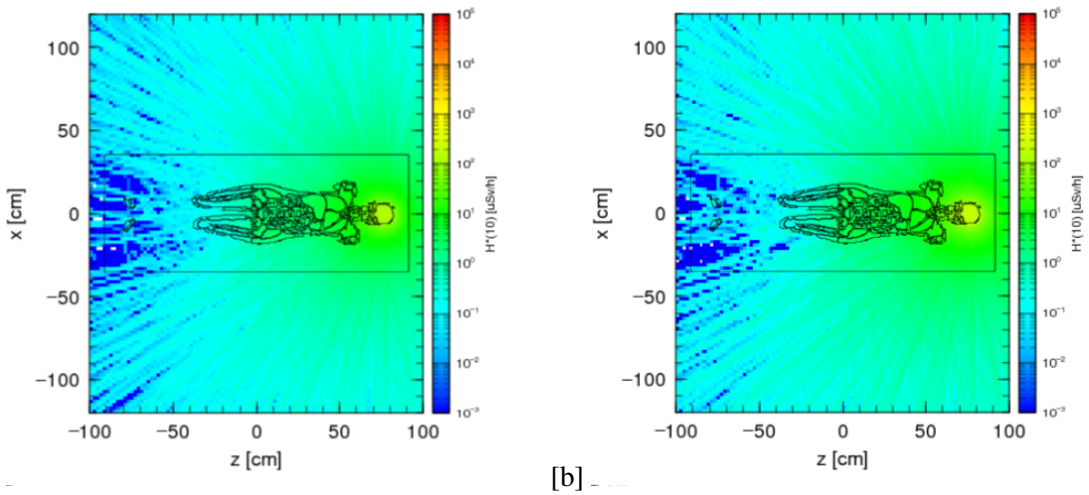

[a] [b]

Figure 2.4: H*(10) maps at 15 minutes after 1 hour [a] and 2 hours [b] of irradiation in the head and neck region.

Table 2.14: H*(10) produced by the patient activation due to irradiation of the head and neck district after 15 minutes.

Radius (cm)	H*(10) 1h irr. (μSv/h)	Rel. err.	H*(10) 2h irr. (μSv/h)	Rel. err.
30-40	$3.21 \cdot 10^{1}$	$1.5 \cdot 10^{-2}$	$5.33 \cdot 10^{1}$	$1.5 \cdot 10^{-2}$
40-50	$2.35 \cdot 10^{1}$	$1.5 \cdot 10^{-2}$	$3.90 \cdot 10^{1}$	$1.5 \cdot 10^{-2}$
50-60	$1.83 \cdot 10^{1}$	$1.5 \cdot 10^{-2}$	$3.03 \cdot 10^{1}$	$1.5 \cdot 10^{-2}$
60-70	$1.47 \cdot 10^{1}$	$1.5 \cdot 10^{-2}$	$2.45 \cdot 10^{1}$	$1.5 \cdot 10^{-2}$
70-80	$1.22 \cdot 10^{1}$	$1.5 \cdot 10^{-2}$	$2.03 \cdot 10^{1}$	$1.5 \cdot 10^{-2}$
80-90	$1.03 \cdot 10^{1}$	$1.5 \cdot 10^{-2}$	$1.71 \cdot 10^{1}$	$1.5 \cdot 10^{-2}$
90-100	8.84	$1.5 \cdot 10^{-2}$	$1.47 \cdot 10^{1}$	$2.0 \cdot 10^{-2}$
100-110	7.65	$1.5 \cdot 10^{-2}$	$1.27 \cdot 10^{1}$	$2.0 \cdot 10^{-2}$
110-120	6.70	$2.0 \cdot 10^{-2}$	$1.11 \cdot 10^{1}$	$2.0 \cdot 10^{-2}$

The values at distances between 30-40cm are especially important because represent the dose that medical staff will absorb assisting the patient. The dose at 100-110cm is interesting because that represents the interpersonal distance. Values between 0cm and 30cm are not reported because in this region the presence of the patient makes invalid the H*(10) as explained above.

Figure 2.5 shows a comparison of the transversal maps of the values reported in table 2.14 for both the irradiation times.

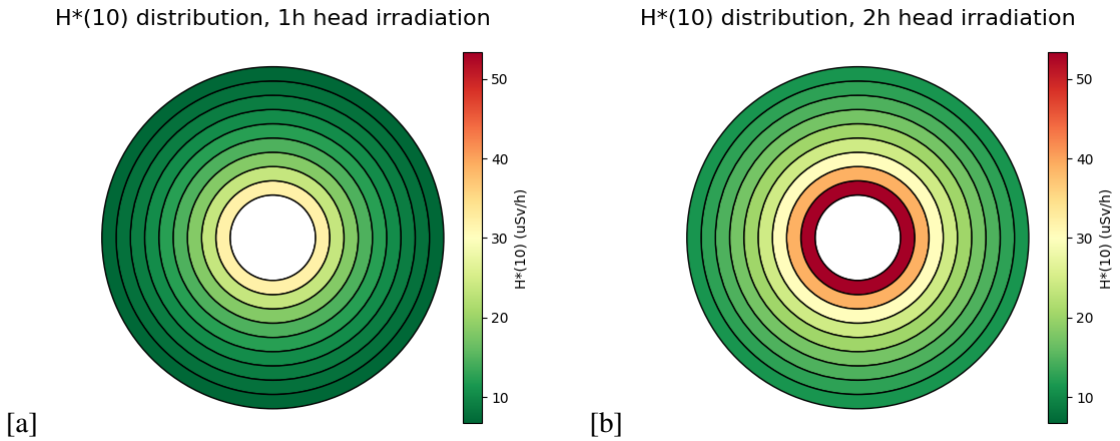

[a] [b]

Figure 2.5: H*(10) transversal maps of the values in 2.14 after 1 hour [a] and 2 hours [b] head irradiation.

2.1.2 Irradiation of the thoracic district

For both the irradiation times for the thorax district, the three regions with a higher activity are:

- N° 10700, trunk muscles;
- N° 11700, trunk residual soft tissues;
- N° 9500, liver.

Figure 2.6 shows the thorax geometry. In particular region 10700 is represented in dark green, region 11700 in light blue and region 9500 in dark brown.

Figure 2.6: Thorax particular.

Table 2.15: Total number of produced γ-rays for both irradiation times at 15 minutes after the shutdown

Region	1h+15m (s^{-1})	Rel. err	2h+15m (s^{-1})	rel. err
10700	$3.20 \cdot 10^6$	1.0%	$5.55 \cdot 10^6$	1.0%
11700	$2.94 \cdot 10^6$	1.0%	$5.08 \cdot 10^6$	1.0%
9500	$1.06 \cdot 10^6$	1.0%	$1.84 \cdot 10^6$	1.0%

In this case the liver is one of the most activated organs. This fact should be considered during the evaluation of the patient positioning. External shielding might be used to lower activation of the out-of-field organs, although activation is also due to internal neutron scattering and diffusion.

Tables 2.16, 2.17, 2.18, 2.19, 2.20,2.21 report, for these regions, the three isotopes with higher total activity for 1 hour irradiation at the end of treatment (+ 0 s) and 15 minutes after the shutdown (+ 15 m).

Table 2.16: Region 10700, 1 h Irradiation + 0 s, statistical uncertainty below 0.5%

Isotope	Activity(Bq)	Relative activity	Half life (s)
^{24m} Na	$1.690 \cdot 10^7$	82.75%	$2.018 \cdot 10^{-2}$
^{38} Cl	$1.935 \cdot 10^6$	9.47%	$2.234 \cdot 10^3$
^{24} Na	$1.017 \cdot 10^6$	4.98%	$5.398 \cdot 10^4$

Table 2.17: Region 10700, 1 h Irradiation + 15 m, statistical uncertainty below 0.5%

Isotope	Activity(Bq)	Relative activity	Half life (s)
^{38} Cl	$1.464 \cdot 10^6$	48.32%	$2.234 \cdot 10^3$
^{24} Na	$1.005 \cdot 10^6$	33.19%	$5.398 \cdot 10^4$
^{42} K	$5.333 \cdot 10^5$	17.60%	$4.450 \cdot 10^4$

Table 2.18: Region 11700, 1 h Irradiation + 0 s, statistical uncertainty below 0.5%

Isotope	Activity(Bq)	Relative activity	Half life (s)
^{24m} Na	$1.603 \cdot 10^7$	85.11%	$2.018 \cdot 10^{-2}$
^{38} Cl	$1.826 \cdot 10^6$	9.70%	$2.234 \cdot 10^3$
^{24} Na	$9.647 \cdot 10^5$	5.12%	$5.398 \cdot 10^4$

Table 2.19: Region 11700, 1 h Irradiation + 15 m, statistical uncertainty below 0.5%

Isotope	Activity(Bq)	Relative activity	Half life (s)
^{38} Cl	$1.381 \cdot 10^6$	58.81%	$2.234 \cdot 10^3$
^{24} Na	$9.562 \cdot 10^5$	40.60%	$5.398 \cdot 10^4$
^{32} P	$9.962 \cdot 10^3$	0.42%	$1.232 \cdot 10^6$

Table 2.20: Region 9500, 1 h Irradiation + 0 s, statistical uncertainty below 0.5%

Isotope	Activity(Bq)	Relative activity	Half life (s)
^{24m} Na	$5.704 \cdot 10^{6}$	84.14%	$2.018 \cdot 10^{-2}$
^{38} Cl	$6.547 \cdot 10^{5}$	9.66%	$2.234 \cdot 10^{3}$
^{24} Na	$3.432 \cdot 10^{5}$	5.07%	$5.398 \cdot 10^{4}$

Table 2.21: Region 9500, 1 h Irradiation + 15 m, statistical uncertainty below 0.5%

Isotope	Activity(Bq)	Relative activity	Half life (s)
^{38} Cl	$4.952 \cdot 10^{5}$	54.63%	$2.234 \cdot 10^{3}$
^{24} Na	$3.398 \cdot 10^{5}$	37.43%	$5.398 \cdot 10^{4}$
^{42} K	$6.691 \cdot 10^{4}$	7.38%	$4.450 \cdot 10^{4}$

In these regions, we find the same isotopes that are activated when simulating the irradiation of the head and neck district, thus the same observations hold. In addition, as listed in Table 2.19, the ^{32}P is present with an activity equal to the 0.42% of the total, with half life τ $1.232 \cdot 10^{6}$ s. This means that, after some days, the activity of the short-half life isotopes will be negligible and the main contribution will come from ^{32}P. However, given its low activity, its contribution will also be negligible.

Tables 2.22, 2.23, 2.24, 2.25, 2.26,2.27 report the three main isotopes for the 2 hour irradiation.

Table 2.22: Region 10700, 2 h Irradiation + 0 s, statistical uncertainty below 0.5%

Isotope	Activity(Bq)	Relative activity	Half life (s)
^{24m} Na	$1.690 \cdot 10^{7}$	74.90%	$2.018 \cdot 10^{-2}$
^{38} Cl	$2.569 \cdot 10^{6}$	11.38%	$2.234 \cdot 10^{3}$
^{24} Na	$1.988 \cdot 10^{6}$	8.81%	$5.398 \cdot 10^{4}$

Table 2.23: Region 10700, 2 h Irradiation + 15 m, statistical uncertainty below 0.5%

Isotope	Activity(Bq)	Relative activity	Half life (s)
^{24} Na	$1.965 \cdot 10^{6}$	39.33%	$5.398 \cdot 10^{4}$
^{38} N	$1.943 \cdot 10^{6}$	38.87%	$2.234 \cdot 10^{3}$
^{42} K	$1.037 \cdot 10^{6}$	20.76%	$4.450 \cdot 10^{4}$

Table 2.24: Region 11700, 2 h Irradiation + 0 s, statistical uncertainty below 0.5%

Isotope	Activity(Bq)	Relative activity	Half life (s)
^{24m} Na	$1.603 \cdot 10^{7}$	78.70%	$2.018 \cdot 10^{-2}$
^{38} Cl	$2.424 \cdot 10^{6}$	11.90%	$2.234 \cdot 10^{3}$
^{24} Na	$1.886 \cdot 10^{6}$	9.24%	$5.398 \cdot 10^{4}$

Table 2.25: Region 11700, 2 h Irradiation + 15 m, statistical uncertainty below 0.5%

Isotope	Activity(Bq)	Relative activity	Half life (s)
^{24} Na	$1.864 \cdot 10^{6}$	50.05%	$5.398 \cdot 10^{4}$
^{38} Cl	$1.833 \cdot 10^{6}$	49.22%	$2.234 \cdot 10^{3}$
^{32} P	$1.990 \cdot 10^{4}$	0.53%	$1.232 \cdot 10^{6}$

Table 2.26: Region 9500, 2 h Irradiation + 0 s, statistical uncertainty below 0.5%

Isotope	Activity(Bq)	Relative activity	Half life (s)
^{24m} Na	$5.704 \cdot 10^{6}$	77.22%	$2.018 \cdot 10^{-2}$
^{38} Cl	$8.689 \cdot 10^{5}$	11.77%	$2.234 \cdot 10^{3}$
^{24} Na	$6.705 \cdot 10^{5}$	9.08%	$5.398 \cdot 10^{4}$

Table 2.27: Region 9500, 2 h Irradiation + 15 m, statistical uncertainty below 0.5%

Isotope	Activity(Bq)	Relative activity	Half life (s)
^{24} Na	$6.632 \cdot 10^{5}$	45.41%	$5.398 \cdot 10^{4}$
^{38} Cl	$6.572 \cdot 10^{5}$	45.00%	$2.234 \cdot 10^{3}$
^{42} K	$1.302 \cdot 10^{5}$	8.91%	$4.450 \cdot 10^{4}$

All the considerations explained above are still valid for the data in these tables.

Figure 2.7 shows the H*(10) maps for thorax at 15 minutes after 1 hour and 2 hours of irradiation time. Also in this case it is clear that the highest contribution to the dose comes from the irradiated district.

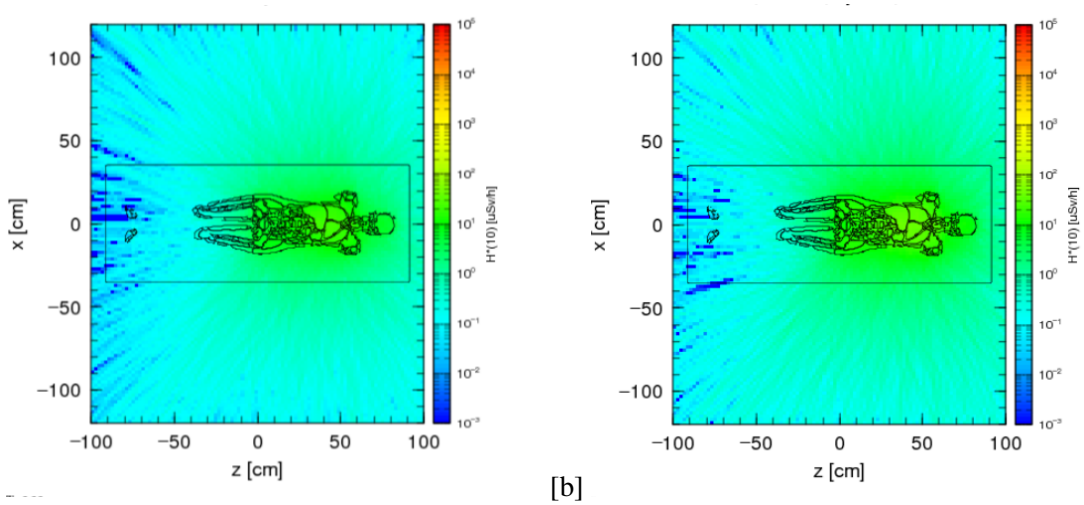

[a] [b]

Figure 2.7: H*(10) maps results at 15 minutes after 1 hour [a] and 2 hours [b] thorax irradiation.

Table 2.28 reports the sum over all the cylindrical mesh height of the H*(10) values for each annulus of the mesh.

Table 2.28: H*(10) produced by the patient activation due to irradiation of the thoracic district at 15 minutes after the beam shutdown.

Radius (cm)	H*(10) 1h irr. (μSv/h)	Rel. err.	H*(10) 2h irr. (μSv/h)	Rel. err.
30-40	$3.27{\cdot}10^{1}$	$1.0{\cdot}10^{-2}$	$5.65{\cdot}10^{1}$	$1.0{\cdot}10^{-2}$
40-50	$2.31{\cdot}10^{1}$	$1.0{\cdot}10^{-2}$	$3.99{\cdot}10^{1}$	$1.5{\cdot}10^{-2}$
50-60	$1.74{\cdot}10^{1}$	$1.5{\cdot}10^{-2}$	$3.00{\cdot}10^{1}$	$1.5{\cdot}10^{-2}$
60-70	$1.36{\cdot}10^{1}$	$1.5{\cdot}10^{-2}$	$2.35{\cdot}10^{1}$	$1.5{\cdot}10^{-2}$
70-80	$1.10{\cdot}10^{1}$	$1.5{\cdot}10^{-2}$	$1.89{\cdot}10^{1}$	$1.5{\cdot}10^{-2}$
80-90	9.04	$1.5{\cdot}10^{-2}$	$1.56{\cdot}10^{1}$	$1.5{\cdot}10^{-2}$
90-100	7.58	$1.5{\cdot}10^{-2}$	$1.31{\cdot}10^{1}$	$1.5{\cdot}10^{-2}$
100-110	6.44	$1.5{\cdot}10^{-2}$	$1.11{\cdot}10^{1}$	$1.5{\cdot}10^{-2}$
110-120	5.54	$1.5{\cdot}10^{-2}$	9.56	$2.0{\cdot}10^{-2}$

Figure 2.8 represents a map of the results reported in table 2.28. This can be useful to make an easy comparison between the two irradiation times and understand the ambient dose at a certain distance from the patient.

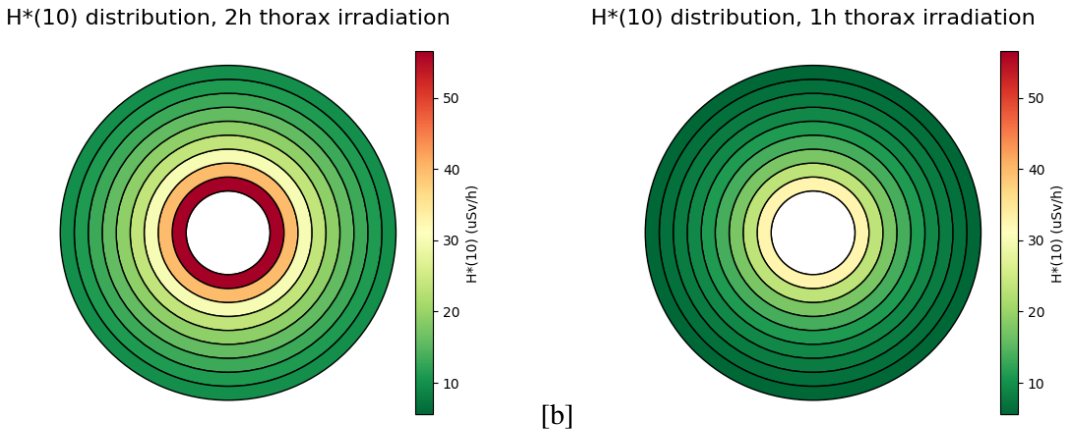

[a] [b]

Figure 2.8: H*(10) transversal maps of the values in 2.28 after 1 hour [a] and 2 hours [b] thorax irradiation.

2.1.3 Irradiation of the lower limbs district

When irradiating the lower limbs, the three regions with a higher activity produced are:

- N° 10900, legs muscles;
- N° 11900, legs residual soft tissues;
- N° 3400, tibia, fibulae and patellae cortical bone.

Figure 2.9 shows a zoom of the lower limb part of the body where the three mentioned regions are visible: region 10900 in dark green, region 11700 in lilac and region 3400 in purple.

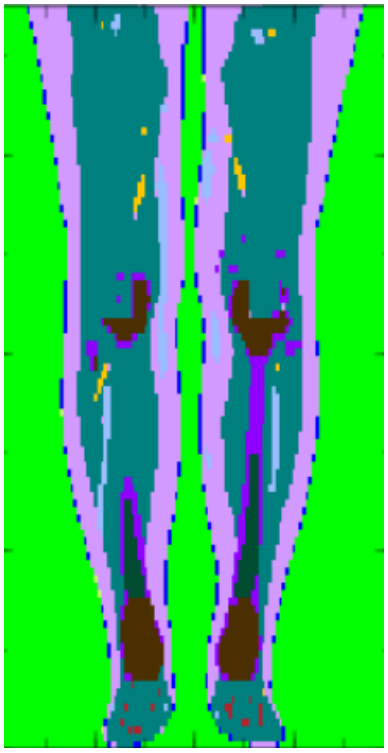

Figure 2.9: Legs geometry particular.

Table 2.29: Total number of γ-rays produced for both irradiation times at 15 minutes after the shutdown

Region	1h+15m (s^{-1})	Rel. err	2h+15m (s^{-1})	Rel. err
10900	$1.69 \cdot 10^{6}$	1.0%	$2.93 \cdot 10^{6}$	1.0%
11900	$1.16 \cdot 10^{6}$	1.0%	$2.01 \cdot 10^{6}$	1.0%
3400	$5.89 \cdot 10^{5}$	1.0%	$9.58 \cdot 10^{5}$	1.0%

In this case the gamma production (Table 2.29) is lower with respect to the previous irradiation configurations due to the fact that the legs are mainly composed by muscles and bones. The muscles have the same composition in the whole body but bones tends to be less active respect to the organs in the other parts of the body due to the materials they are made of.

Tables 2.30, 2.31, 2.32, 2.33, 2.34,2.35 report the three main isotopes for 1 hour irradiation at the beam shutdown (+ 0 s) and after 15 minutes (+ 15 m).

Table 2.30: Region 10900, 1 h Irradiation + 0 s, statistical uncertainty below 0.5%

Isotope	Activity(Bq)	Relative activity	Half life (s)
^{24m} Na	$8.924 \cdot 10^{6}$	82.75%	$2.018 \cdot 10^{-2}$
^{38} Cl	$1.022 \cdot 10^{6}$	9.48%	$2.234 \cdot 10^{3}$
^{24} Na	$5.369 \cdot 10^{5}$	4.98%	$5.398 \cdot 10^{4}$

Table 2.31: Region 10900, 1 h Irradiation + 15 m, statistical uncertainty below 0.5%

Isotope	Activity(Bq)	Relative activity	Half life (s)
^{38} Cl	$7.731 \cdot 10^{5}$	48.34%	$2.234 \cdot 10^{3}$
^{24} Na	$5.308 \cdot 10^{5}$	33.19%	$5.398 \cdot 10^{4}$
^{42} K	$2.807 \cdot 10^{5}$	17.55%	$4.450 \cdot 10^{4}$

Table 2.32: Region 11900, 1 h Irradiation + 0 s, statistical uncertainty below 0.5%

Isotope	Activity(Bq)	Relative activity	Half life (s)
^{24m} Na	$6.332 \cdot 10^{6}$	85.13%	$2.018 \cdot 10^{-2}$
^{38} Cl	$7.193 \cdot 10^{5}$	9.67%	$2.234 \cdot 10^{3}$
^{24} Na	$3.810 \cdot 10^{5}$	5.12%	$5.398 \cdot 10^{4}$

Table 2.33: Region 11900, 1 h Irradiation + 15 m, statistical uncertainty below 0.5%

Isotope	Activity(Bq)	Relative activity	Half life (s)
^{38} Cl	$5.440 \cdot 10^{5}$	58.74%	$2.234 \cdot 10^{3}$
^{24} Na	$3.766 \cdot 10^{5}$	40.66%	$5.398 \cdot 10^{4}$
^{32} P	$3.925 \cdot 10^{3}$	0.42	$1.232 \cdot 10^{6}$

Table 2.34: Region 3400, 1 h Irradiation + 0 s, statistical uncertainty below 0.5%

Isotope	Activity(Bq)	Relative activity	Half life (s)
^{24m} Na	$3.287 \cdot 10^{6}$	72.24%	$2.018 \cdot 10^{-2}$
^{49} Ca	$6.795 \cdot 10^{5}$	14.94%	$5.231 \cdot 10^{2}$
^{49} Sc	$2.956 \cdot 10^{5}$	6.50%	$3.431 \cdot 10^{3}$

Table 2.35: Region 3400, 1 h Irradiation + 15 m, statistical uncertainty below 0.5%

Isotope	Activity(Bq)	Relative activity	Half life (s)
^{49} Sc	$3.113 \cdot 10^{5}$	39.51%	$3.431 \cdot 10^{3}$
^{49} Ca	$2.062 \cdot 10^{5}$	26.17%	$5.231 \cdot 10^{2}$
^{24} Na	$1.955 \cdot 10^{5}$	24.81%	$5.398 \cdot 10^{4}$

The relative activity for the regions 10900 and 11900 is almost equal, respectively, to the one for the cells 10700 and 11700 in the case of thorax irradiation due to the fact that these cells are composed by the same material. The absolute activity instead is different due to the different shape and quantity of irradiated material. Region 3400 instead has the same composition of region 2600, so also in this case the activated isotopes are the same.

Tables 2.36, 2.37, 2.38, 2.39, 2.40,2.41 report the three main isotopes for 2 hour irradiation.

Table 2.36: Region 10900, 2 h Irradiation + 0 s, statistical uncertainty below 0.5%

Isotope	Activity(Bq)	Relative activity	Half life (s)
^{24m} Na	$8.924 \cdot 10^{6}$	74.91%	$2.018 \cdot 10^{-2}$
^{38} Cl	$1.357 \cdot 10^{6}$	11.39%	$2.234 \cdot 10^{3}$
^{24} Na	$1.050 \cdot 10^{6}$	8.81%	$5.398 \cdot 10^{4}$

Table 2.37: Region 10900, 2 h Irradiation + 15 m, statistical uncertainty below 0.5%

Isotope	Activity(Bq)	Relative activity	Half life (s)
^{24} Na	$1.038 \cdot 10^{6}$	39.34%	$5.398 \cdot 10^{4}$
^{38} Cl	$1.026 \cdot 10^{6}$	38.90%	$2.234 \cdot 10^{3}$
^{42} K	$5.460 \cdot 10^{5}$	20.70%	$4.450 \cdot 10^{4}$

Table 2.38: Region 11900, 2 h Irradiation + 0 s, statistical uncertainty below 0.5%

Isotope	Activity(Bq)	Relative activity	Half life (s)
^{24m} Na	$6.332 \cdot 10^{6}$	78.73%	$2.018 \cdot 10^{-2}$
^{38} Cl	$9.548 \cdot 10^{5}$	11.87%	$2.234 \cdot 10^{3}$
^{24} Na	$7.448 \cdot 10^{5}$	9.26%	$5.398 \cdot 10^{4}$

Table 2.39: Region 11900, 2 h Irradiation + 15 m, statistical uncertainty below 0.5%

Isotope	Activity(Bq)	Relative activity	Half life (s)
^{24} Na	$7.363 \cdot 10^{5}$	50.11%	$5.398 \cdot 10^{4}$
^{38} Cl	$7.221 \cdot 10^{5}$	49.14%	$2.234 \cdot 10^{3}$
^{32} P	$7.842 \cdot 10^{3}$	0.53%	$1.232 \cdot 10^{6}$

Table 2.40: Region 3400, 2 h Irradiation + 0 s, statistical uncertainty below 0.5%

Isotope	Activity(Bq)	Relative activity	Half life (s)
^{24m} Na	$3.287 \cdot 10^{6}$	65.57%	$2.018 \cdot 10^{-2}$
^{49} Ca	$6.853 \cdot 10^{5}$	13.67%	$5.231 \cdot 10^{2}$
^{49} Sc	$4.965 \cdot 10^{5}$	9.91%	$3.431 \cdot 10^{3}$

Table 2.41: Region 3400, 2 h Irradiation + 15 m, statistical uncertainty below 0.5%

Isotope	Activity(Bq)	Relative activity	Half life (s)
^{49} Sc	$4.793 \cdot 10^5$	39.56%	$3.431 \cdot 10^3$
^{24} Na	$3.821 \cdot 10^5$	31.54%	$5.398 \cdot 10^4$
^{49} Ca	$2.079 \cdot 10^5$	17.16%	$5.231 \cdot 10^2$

These isotopes are the same as in the other irradiation positions so the same conclusions are still valid.

As a future work, it will be interesting to repeat the evaluation in presence of prosthesis, for example titanium hips, which can increase the produced activity and so the H*(10).

Figure 2.10 represents the H*(10) map for the lower limbs district irradiation at 15 minutes after 1 hour and 2 hours irradiation.

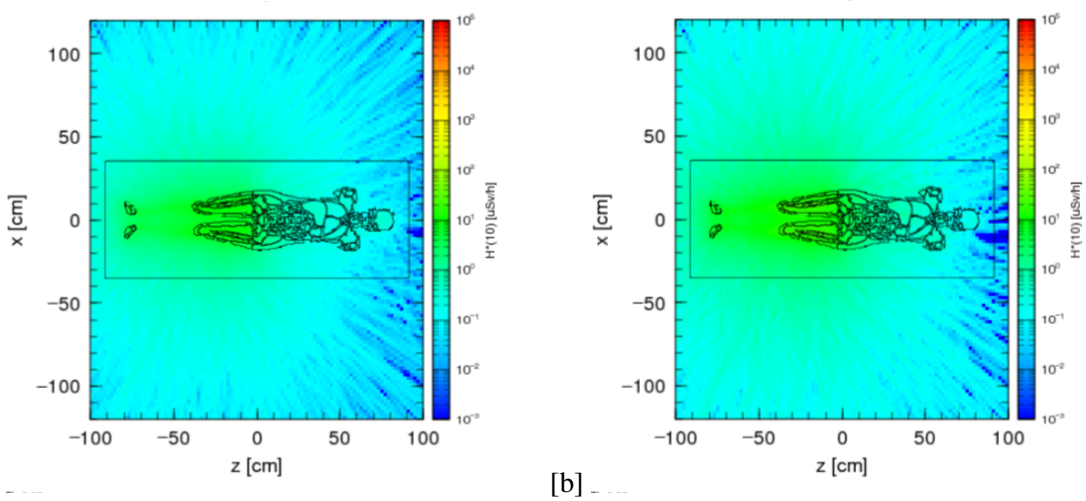

[a] [b]

Figure 2.10: H*(10) maps results at 15 minutes after 1 hour [a] and 2 hours [b] legs irradiation.

Table 2.42 reports the values of the equivalent ambient dose produced by the patient activation due to the lower limbs district irradiation in a radius of 120 cm. The results in this table are graphically reported in Fig. 2.11 which shows the transversal maps of H*(10) around the patient.

Table 2.42: H*(10) produced by the patient activation due to legs irradiation after 15 minutes

Radius (cm)	H*(10) 1h irr. (μSv/h)	Rel. err.	H*(10) 2h irr. (μSv/h)	Rel. err.
30-40	$1.84{\cdot}10^{1}$	$1.0{\cdot}10^{-2}$	$3.17{\cdot}10^{1}$	$1.0{\cdot}10^{-2}$
40-50	$1.31{\cdot}10^{1}$	$1.0{\cdot}10^{-2}$	$2.26{\cdot}10^{1}$	$1.5{\cdot}10^{-2}$
50-60	9.93	$1.5{\cdot}10^{-2}$	$1.71{\cdot}10^{1}$	$1.5{\cdot}10^{-2}$
60-70	7.80	$1.5{\cdot}10^{-2}$	$1.34{\cdot}10^{1}$	$1.5{\cdot}10^{-2}$
70-80	6.30	$1.5{\cdot}10^{-2}$	$1.08{\cdot}10^{1}$	$1.5{\cdot}10^{-2}$
80-90	5.19	$1.5{\cdot}10^{-2}$	8.93	$1.5{\cdot}10^{-2}$
90-100	4.33	$1.5{\cdot}10^{-2}$	7.46	$1.5{\cdot}10^{-2}$
100-110	3.68	$1.5{\cdot}10^{-2}$	6.33	$1.5{\cdot}10^{-2}$
110-120	3.16	$1.5{\cdot}10^{-2}$	5.45	$1.5{\cdot}10^{-2}$

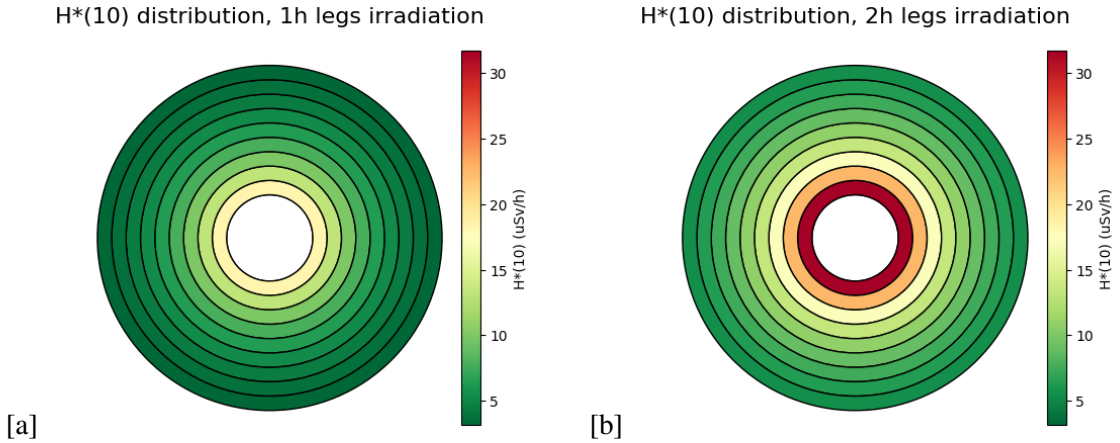

[a] [b]

Figure 2.11: H*(10) transversal maps of the values in Table 2.42 after 1 hour [a] and 2 hours [b] legs irradiation

2.1.4 Comparison with ^{131}I

Knowing the distribution of H*(10) due to the patient activation at each different position, it is now possible to evaluate the impact of these results by comparison to what obtained in Chapter 1 for the 600MBq ^{131}I administration.

Table 2.43 reports the values obtained in the simulations at two meaningful distances: 30-40 cm which represents the average distance between patient and hospital staff during the post-treatment phase and 100-110 cm, representing the interpersonal distance in normal interactions. In order to maintain these considerations as conservative as possible, the comparison was carried out with the 2 hours irradiation case, despite it is not the most realistic situation.

Table 2.43: H*(10) comparison between Iodine administration and irradiation induced dose at 15 minutes after 2h irradiation. The statistical uncertainty is lower than 2%.

Radius (cm)	^{131}I (μSv/h)	Head (μSv/h)	Thorax (μSv/h)	Legs (μSv/h)
30-40	$1.15{\cdot}10^{3}$	$5.33{\cdot}10^{1}$	$5.65{\cdot}10^{1}$	$3.17{\cdot}10^{1}$
100-110	$2.49{\cdot}10^{2}$	$1.27{\cdot}10^{1}$	$1.11\cdot10^{1}$	6.33

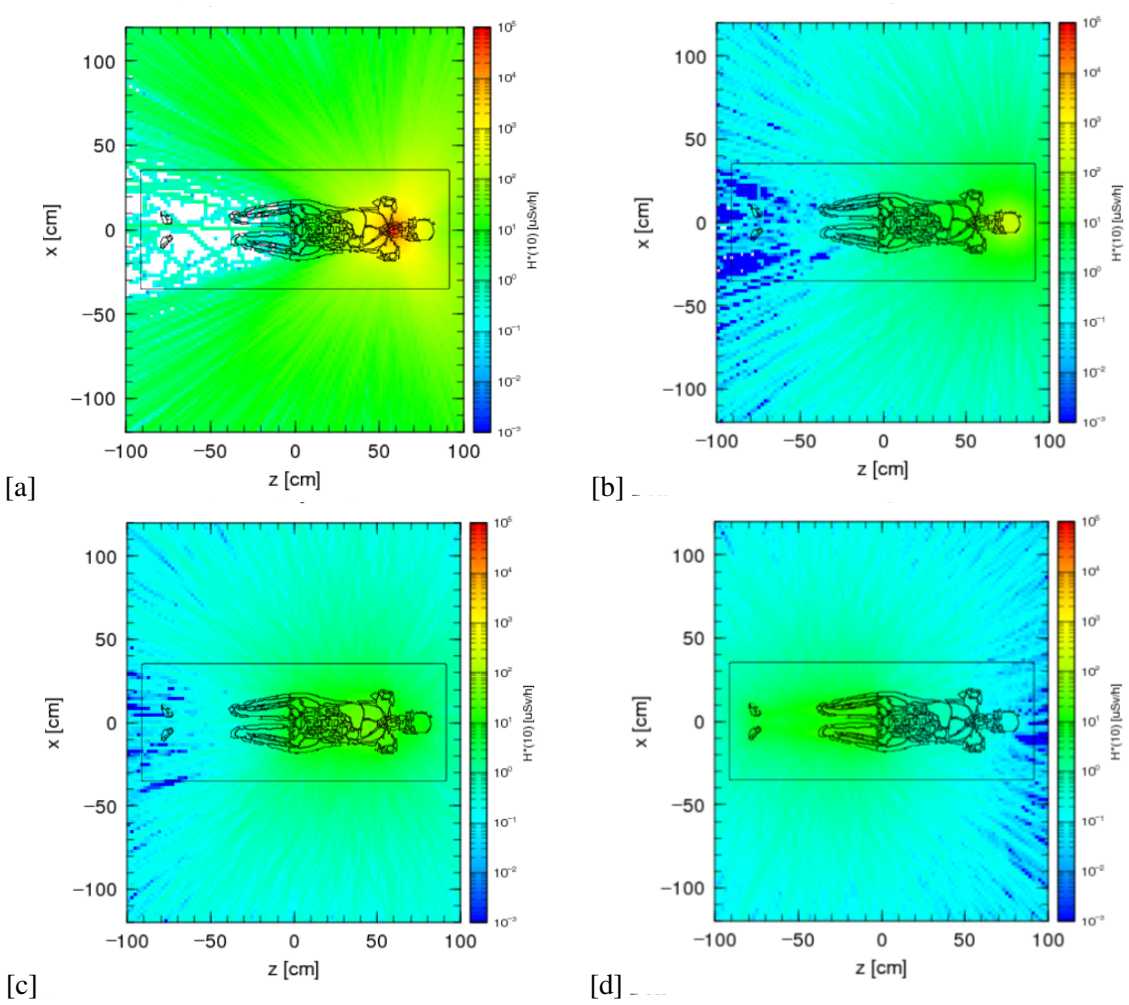

Figure 2.12: H*(10) maps due to ^{131}I administration [a] and due to 2 hours irradiation activation (after 15 minutes) for head [b], thorax [c], legs [d].

Figure 2.12 shows the H*(10) maps due to 600 MBq of iodine in the thyroid, and the H*(10) at 15 minutes after the end of irradiation of the three districts described above.

From Table 2.43 and Figure 2.12 it is evident that the iodine produces a higher ambient dose with respect to the neutron irradiation even in the most conservative assumptions. The difference is almost of two order of magnitude at 15 minutes after 2 hours irradiation. This means that, from

the radiation protection point of view, the patient could be discharged already after 15 minutes post irradiation. In other BNCT centres treating patients, after the irradiation patients are kept in a dedicated room for one hour to observe the general conditions, allow for rest and wait for activation cooling. In Xiamen (China), the activation of patients is monitored with a germanium detector and from discussion with the medical physicists responsible of the patients management, the results obtained by the described calculations are compatible with what observed in their experience. Thus, at the moment of patients discharge, the dose due to patient irradiation will be even lower and it will not constitute a radiation protection issue.

2.1.5 Urine activation

To produce the executive plan of the facility and in view of its commissioning, the evaluation of the activation of urine is a necessary step in order to plan their disposal. All the activated excretions must be in fact collected in special shielded containers waiting for the decay and the activity reduction. To obtain values as precise as possible it is necessary to describe the urine with a composition as realistic as possible. The bladder urinary content provided in the phantom from [25] - cell (N° 13800) - lacks of some elements like chlorine and sulfur that are relevant for activation analysis. The latter is interesting because of the reaction ^{34}S(n,γ)^{35}S and the following production of ^{35}S with a half-life of 87.5 days [28].

For this reason I have changed the urine composition in the `MCRP-AF.material` file according to [29] as reported in table 2.44.

	H	C	N	O	Na	P	S	Cl	K
Default	10.7	0.3	1	87.1	0.4	0.1	-	-	0.2
New	10.978	0.499	0.988	86.0276	0.3992	0.998	0.2	0.5988	0.1996

Table 2.44: Urine composition in percentage.

At the end of the irradiation, for both 1 hour and 2 hour irradiations, the highest contribution to the activity ($\tilde{7}3\%$ at 1h and $\tilde{8}0\%$ at 2h for all the irradiation positions) is given by the ^{24m}Na. The half-life of this isotope is $2.018 \cdot 10^{-2}$ s, hence its activity is significantly reduced already one second after the beam shutdown.

Tables 2.45,2.46, 2.47 report the three most activated isotopes for each position and at 1 second after 1 hour and 2 hours of irradiation. For this evaluation I have chosen a time interval of 1 second as the reference because in this case there is not a representative situation as the typical waiting time before entrance of staff in the room. Choosing 1 second instead of 0 seconds (i.e. the moment that the beam is shut down), is also justified to avoid the inclusion of the high contribution of ^{24m}Na, which becomes negligible in fractions of seconds after the irradiation because of its very short half-life. In addition, the activity of ^{35}S is reported because of its relevance due to its long half life. For this isotope, together with the relative activity, it is also reported its position among the most activated elements.

Table 2.45: Most relevant isotopes activated in the irradiation of the head and neck district. Statistical uncertainty is below 4.5%

Head	1h activity (Bq)	Relative activity	2h activity (Bq)	Relative activity	Half-life (s)
^{38}Cl	$8.801 \cdot 10^{2}$	71.92%	$1.169 \cdot 10^{3}$	63.91%	$2.234 \cdot 10^{3}$
^{24}Na	$3.085 \cdot 10^{2}$	25.18%	$6.030 \cdot 10^{2}$	32.97%	$5.398 \cdot 10^{4}$
^{42}K	$2.034 \cdot 10^{1}$	1.66%	$3.957 \cdot 10^{1}$	2.16%	$4.450 \cdot 10^{4}$
^{35}S	1.545	0.13% (5°)	3.089	0.17% (5°)	$7.561 \cdot 10^{6}$

Table 2.46: Most relevant isotopes activated in the irradiation of the thoracic district. Statistical uncertainty is below 4%.

Head	1h activity (Bq)	Relative activity	2h activity (Bq)	Relative activity	Half-life (s)
^{38}Cl	$3.440 \cdot 10^{3}$	72.49%	$4.451 \cdot 10^{3}$	64.27%	$2.234 \cdot 10^{3}$
^{24}Na	$1.203 \cdot 10^{3}$	25.37%	$2.353 \cdot 10^{3}$	33.12%	$5.398 \cdot 10^{4}$
^{42}K	$7.910 \cdot 10^{1}$	1.67%	$1.539 \cdot 10^{1}$	2.17%	$4.450 \cdot 10^{4}$
^{35}S	6.049	0.13% (5°)	$1.209 \cdot 10^{1}$	0.17% (5°)	$7.561 \cdot 10^{6}$

Table 2.47: Most relevant isotopes activated in the irradiation of the lower limbs district. Statistical uncertainty is below 3.5%.

Head	1h activity (Bq)	Relative activity	2h activity (Bq)	Relative activity	Half-life (s)
^{38}Cl	$7.996 \cdot 10^{3}$	72.61%	$1.061 \cdot 10^{4}$	64.34%	$2.234 \cdot 10^{3}$
^{24}Na	$2.796 \cdot 10^{3}$	25.39%	$5.466 \cdot 10^{3}$	33.14%	$5.398 \cdot 10^{4}$
^{42}K	$1.841 \cdot 10^{2}$	1.67%	$3.583 \cdot 10^{2}$	2.17%	$4.450 \cdot 10^{4}$
^{35}S	$1.401 \cdot 10^{1}$	0.13% (4°)	$2.802 \cdot 10^{1}$	0.17% (4°)	$7.561 \cdot 10^{6}$

Among the listed isotopes also ^{40}K is relevant, whit an activity that goes from some Bq (in the irradiation of the head and neck region) to a tenth of Bq (in the irradiation of the lower limbs). This isotope is interesting because of its really long half-life (10^{9} years). This means that its activity will be unchanged over the time of stocking in the containers. The conclusion of this analysis is that, after about ten days, the main contributions will come from the ^{35}S and ^{40}K.

Table 2.48 shows the total and the specific (per unit gram) urine activity for each irradiation time and position at 1 second after the irradiation. It is clear that the irradiation of the lower limbs district causes a higher activation of the urine because of the higher neutron flux in the bladder. Also in this case, the effect of external shields could be tested as possible countermeasures to decrease bladder content activation.

	Head 1h	Head 2h
Activity (Bq)	$1.225 \cdot 10^3$ (3%)	$1.829 \cdot 10^3$ (3%)
Specific activity (Bq/g)	6.13	9.15

	Thorax 1h	Thorax 2h
Activity (Bq)	$4.747 \cdot 10^3$ (3%)	$7.103 \cdot 10^3$(3%)
Specific activity (Bq/g)	23.74	35.52

	Legs 1h	Legs 2h
Activity (Bq)	$1.103 \cdot 10^4$ (2%)	$1.649 \cdot 10^4$(2%)
Specific activity (Bq/g)	55.07	82.45

Table 2.48: Urine activity for each irradiation position. In brackets is reported the statistical uncertainty in percentage.

Chapter 3

Activation of the Beam Shaping Assembly.

Based on the experience of other BNCT clinical centres, using neutron beams of similar spectra and intensity, the patient must wait a tenth of minutes in the irradiation room after the treatment ends and before the medical staff enters the room. In this waiting time in the irradiation position, the patient would be subject to a source of radiation due to the BSA activation. In this Chapter I consider different strategies to avoid this undesired exposition.

To calculate the dose absorbed by patient due to this source, it is necessary to know the BSA composition, its activation and the relative γ-emission.

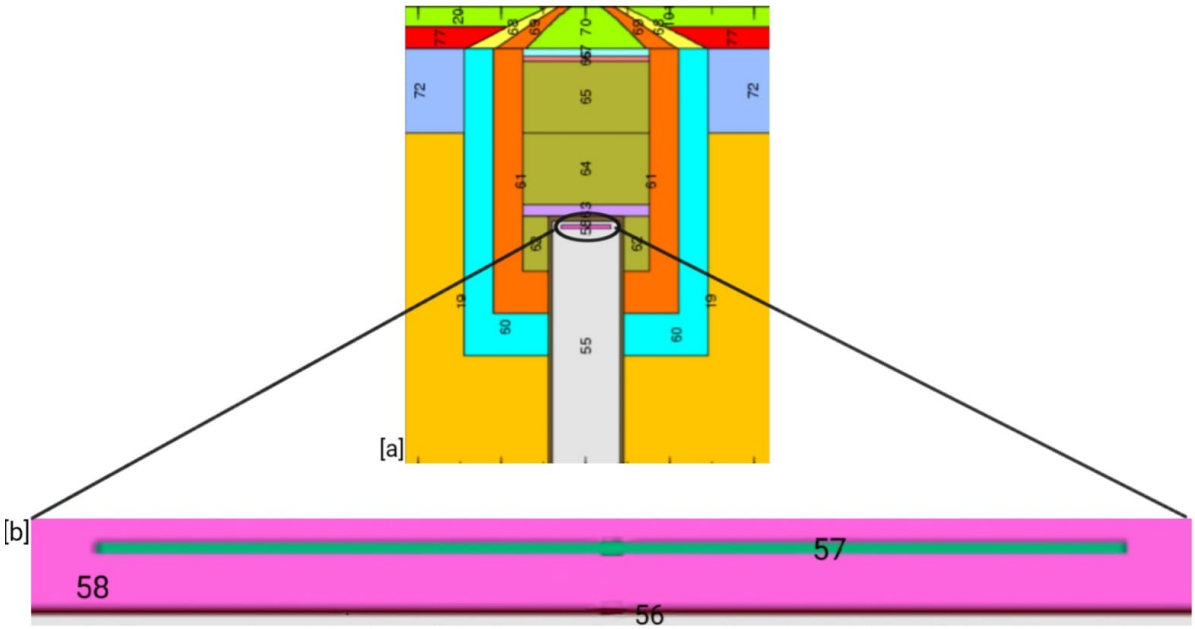

Figure 3.1: Simulated BSA composition [a], target particular [b].

Figure 3.1 shows the composition of BSA in its preliminary configuration. Albeit the inner arrangement of materials and geometry might change to optimize the beam for the treatment, the materials are very representative of the final design. Each number in the image is associated to a material with a specific function:

- N° 54, beam line steel,
- N° 55, beam void;
- N° 56, Be target;
- N° 57, Va layer;
- N° 58, Cu layer;
- N° 60, polyethylene shield;
- N° 61, Pb reflector;
- N° 62, back reflector moderator (AlF_3);
- N° 63, fast neutrons filter (Fe);
- N° 64-65, moderators (AlF_3);
- N° 66, γ-filter (Bi);
- N° 67, thermal neutrons filter (LiF);
- N° 68, neutron shield (polyethylene Li);
- N° 69,γ-shield (Pb).

The target, zoomed in Figure 3.1 [b], is simulated according to the information provided by [30]. Close to the beam there is the beryllium layer, region 56, for the neutron production. The fuchsia region, number 58, is made by copper and it is used for the heat removal. Region 57 is a thin Vanadium layer that, thanks to its high permeability to molecular hydrogen, is used to avoid the blistering. This is the formation of bubbles of gaseous hydrogen that would be trapped into beryllium, whose permeation to gas is very poor, that can damage the target.

As anticipated above, this version of the BSA is not the definitive one. A previous design had been published before in [8], but currently it is being re-designed to take in account some improvement in the target which allows to extract the neutron beam in the forward direction, and improving the engineering in view of its construction. Anyway, the BSA shown in Figure 3.1 is representative for the purposes of this thesis. In fact to evaluate its activation and the consequent dose it is important to know the materials composing it. The BSA is an ensemble of moderating, absorbent and reflective materials with the function of obtaining a epithermal neutron beam and reducing the out-of-field dose. The idea is to suppress the thermal and fast neutron contamination and the gamma dose down to acceptable levels as recommended by the IAEA guidelines [5]. Materials such as lead and bismuth are used as gamma absorbers, while iron is used as a fast neutron filter. To absorb thermal neutron, lithium is present in different parts of the BSA. The combination of AlF_3 and LiF, a material called Alliflu [28], has been sintered in Pavia. It has been proved to be

the best option to tailor the epithermal neutron beam while ensuring a high flux. Polyethylene and lead are used to avoid the escape respectively of neutrons and gamma from the BSA to the walls. The absorption of neutrons by hydrogenated materials help, in turn, to reduce the activation and the ambient dose. Regions from 62 to 67 are used to moderate and filter the beam to obtain a suitable neutron spectrum and reduce the contamination. Regions 68 and 69 collimate the beam.

Table 3.1: Total number of γ-rays produced in the BSA activated regions at 1 second and 15 minutes after a 1-hour irradiation. Statistical uncertainty is lower than 2%.

Region	γ-production at 1 s (s^{-1})	γ-production at 15 min (s^{-1})
64	1.05×10^{12}	7.89×10^{9} (2°)
62	8.94×10^{11}	6.80×10^{9} (3°)
65	4.61×10^{11}	3.81×10^{9} (4°)
58	2.05×10^{10}	1.15×10^{10} (1°)
57	2.70×10^{9}	1.68×10^{8} (5°)
67	6.27×10^{8}	7.94×10^{-5} (10°)
61	2.04×10^{7}	1.64×10^{7} (6°)
63	8.63×10^{6}	8.45×10^{6} (7°)
70	3.28×10^{4}	2.98×10^{4} (8°)
69	2.41×10^{3}	6.86×10^{2} (9°)

Table 3.1 shows the produced γ-rays region by region at 1 second and 15 minutes after a 1-hour irradiation listed from the highest to the lowest value at 1 second. These values are used to write the input source files used to calculate H*(10). For each region, the file `spd-act` contains the total activity, comprising each decay mode, for each isotope present. This can be useful to consider the half-lives of each contribution and have an idea of the time evolution of the activity. These values are shown in Tables 3.2, 3.3, 3.4, 3.5, 3.6,3.7, 3.8, 3.9.

Table 3.2: Isotopes activated in region 64 at 1 second after 1-hour irradiation. Statistical uncertainty < 0.5%.

Isotope	Activity (Bq)	Relative activity (%)	Half-life (s)
^{28} Al	8.278×10^{11}	78.02	1.345×10^{2}
^{20} F	2.303×10^{11}	21.70	1.116×10^{1}

Table 3.3: Isotopes activated in region 62 at 1 second after 1-hour irradiation. Statistical uncertainty < 0.5%.

Isotope	Activity (Bq)	Relative activity (%)	Half-life (s)
^{28} Al	7.163×10^{11}	78.78	1.345×10^{2}
^{20} F	1.861×10^{11}	20.47	1.116×10^{1}

Table 3.4: Isotopes activated in region 65 at 1 second after 1-hour irradiation. Statistical uncertainty < 0.5%.

Isotope	Activity (Bq)	Relative activity (%)	Half-life (s)
^{28} Al	4.033×10^{11}	85.77	1.345×10^{2}
^{20} F	6.683×10^{10}	14.21	1.116×10^{1}

Table 3.5: Isotopes activated in region 58 at 1 second after 1-hour irradiation. Statistical uncertainty < 1%.

58	Activity (Bq)	Relative activity (%)	Half-life (s)
^{66} Cu	1.207×10^{11}	80.70	3.072×10^{2}
^{64} Cu	2.888×10^{10}	19.30	4.570×10^{4}

Tables 3.2, 3.3, 3.4 are relative to regions 64, 62 and 65 which, at 1 second after the irradiation, are the most activated. These are made up of the same material, AlF_3, and so the most radioactive isotopes are the same, ^{28}Al and ^{20}F. Their half-lives are relative short, the longest one is of the order of few minutes, so activity will decrease in short time. This explains why, in table 3.1, at 15 minutes after the irradiation, the most activated region is n°58 The isotopes activated in this region are in table 3.5. ^{64}Cu has a half-life of about 12h and so this contribution will become dominant in few minutes after the irradiation.

Table 3.6: Isotopes activated in region 57 at 1 second after 1-hour irradiation. Statistical uncertainty < 1%.

Isotope	Activity (Bq)	Relative activity (%)	Half-life (s)
^{52} V	2.700×10^{9}	100	2.246×10^{2}

Table 3.6 show the activation of the Vanadium layer in the target. The only isotope activated is ^{52}V which has a half-life of about 4 minutes.

Table 3.7: Isotopes activated in region 67 at 1 second after 1-hour irradiation. Statistical uncertainty < 1%.

Isotope	Activity (Bq)	Relative activity (%)	Half-life (s)
^{20} F	6.052×10^{8}	63.87	1.116×10^{1}
^{8} Li	3.330×10^{8}	35.15	8.399×10^{-1}

Table 3.7 shows the activation in region 67, which is interesting because the γ-activity decreases of 13 orders of magnitude in 15 minutes due to the short half-life of its isotopes . Looking at the total activity, that considers all the decay modes, at 15 minutes it is 8.160×10^{6} Bq and it is all due to the tritium β decay produced by the ^{6}Li(n,α)^{3}H reaction. This is the reaction that makes this material a good choice as a thermal neutron filter. Because of the short range of the products

and thanks to the fact that it remains trapped in the material the ^{3}H activity is not a concern in terms of ambient dose.

Table 3.8: Isotopes activated in region 61 at 1 second after 1-hour irradiation. Statistical uncertainty < 0.5%.

Isotope	Activity (Bq)	Relative activity (%)	Half-life (s)
^{209} Pb	4.295×10^{9}	98.04	1.171×10^{4}

In region 61 the relevant element is lead (Table 3.8). Due to its half-life of about 3h ^{209}Pb, will behave like ^{64}Cu in region 58 and will be one of the highest long-term contributions.

Table 3.9: Isotopes activated in region 63 at 1 second after 1-hour irradiation. Statistical uncertainty < 1%.

Isotope	Activity (Bq)	Relative activity (%)	Half-life (s)
^{55} Fe	7.224×10^{6}	52.84	8.660×10^{7}
^{59} Fe	5.230×10^{6}	38.26	3.844×10^{6}
^{54} Mn	7.143×10^{5}	5.23	2.696×10^{7}

In region 63, at the end of the irradiation, the activity is lower respect to other regions but the activated isotopes have long half-lives (Table 3.9). The longest half-life is of the order of few years and belongs to the most active isotope in this region. After some weeks all the isotopes in the previous regions will decay and the highest activity contribution will come from region 63. It is important to specify that for the purposes of this thesis this is not very relevant because when the patient is inside the room the activity is dominated by the other regions. Anyway this result can be interesting for the maintenance. In fact, the target needs to be replaced after a certain time, because it will be subjected to a high proton current and will undergo a significant heat stress. The BSA will be opened and the target extracted. This means that it is important to predict the activity is present in the BSA and in the target structure itself. Moreover, this kind of analysis is important for the radioactive materials disposal during the BSA decommissioning. Since the material in region 63 has a relatively high activity and a long half-life it might be advisable to evaluate alternatives.

The analysis described so far led to the definition of the radiation source to which patients are exposed after the end of the treatment when staying in front of the beam-port. Because this is unwanted, non-selective absorbed dose, a strategy for a safer option must be put in place. Two sources from the `out-phits` file relative to the BSA activation were created, one at 1 second and one at 15 minutes after the irradiation stop. Then I have evaluated H*(10) in different possible situations:

- Patient is moved away from the BSA, in another location of the treatment room (Fig. 3.2);
- A shutter is placed in front of the beam-port at the end of the irradiation to reduce the radiation reaching the patient, who remains in the irradiation position (Fig. 3.3);

- Both previous strategies put in place.

In order to choose a different position for the patient, away from the beam-port, a possible option is to find the area where the gamma flux is lower. Thus, a feasible solution could be close to the wall of BSA (Fig. 3.2). In the real situation, the movement is done using a robot, as further described in the next Chapter. Regarding the shutter, a lead block with section 20cm $\times$ 20cm and 5cm thick was simulated in front of the beam-port (Figure 3.3).

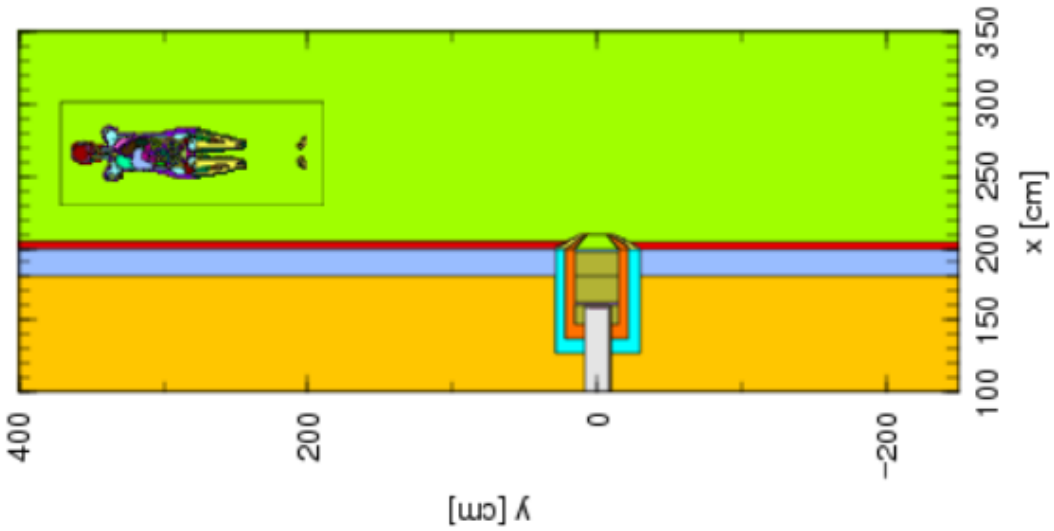

Figure 3.2: New position of the patient after the treatment.

To understand which is the best solution I have evaluated H*(10) for the three conditions, both in the whole room and in the new position where the patient should be located. I have repeated this simulation at 1 second and 15 minutes after 1 hour irradiation.

Table 3.10: H*(10) mean values in the patient position at 1s after 1h irradiation for the three considered conditions: 1) patient moved without shutter, 2) shutter in front of the beam-port, 3) patient moved and shutter in front of the beam-port.

Condition 1		Condition 2		Condition 3	
H*(10) (μSv/h)	Rel. err.	H*(10) (μSv/h)	Rel. err.	H*(10) (μSv/h)	Rel. err.
$4.87 \cdot 10^{1}$	9%	$9.72 \cdot 10^{3}$	0.9%	$4.18 \cdot 10^{1}$	10%

Table 3.10 reports the results of the calculations. It is clear that the mere use of the shutter is not enough to avoid the increase of the absorbed dose due to the activation of the BSA. In fact the difference between this case and the other conditions, in which the patient is moved away from the irradiation position, is about two orders of magnitude. Regarding condition 1 and condition 3 it can be noticed that the presence of the shutter has a little effect on the total dose to the patient immediately after the end of the treatment.

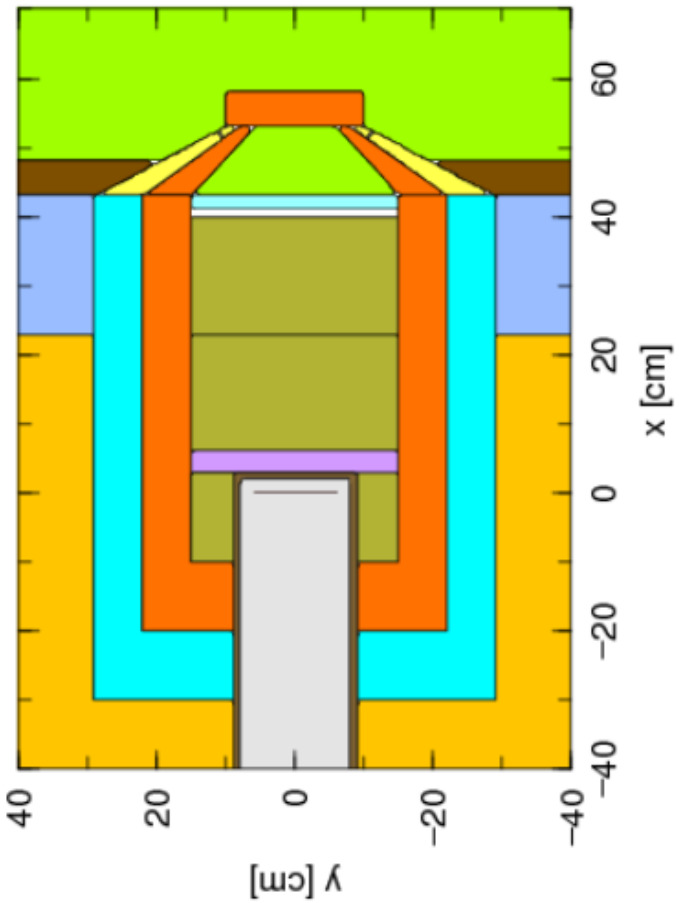

Figure 3.3: BSA with shutter.

Table 3.11: H*(10) mean values in the patient position at 15 minutes after 1h irradiation for the three considered condition: 1) patient moved without shutter, 2) shutter in front of the beam-port, 3) patient moved and shutter in front of the beam-port.

Condition 1		Condition 2		Condition 3	
H*(10) (μSv/h)	Rel. err.	H*(10) (μSv/h)	Rel. err.	H*(10) (μSv/h)	Rel. err.
$3.94 \cdot 10^{-1}$	10%	$7.45 \cdot 10^{1}$	1%	$3.29 \cdot 10^{-1}$	10%

Table 3.11 shows H*(10) for the three conditions at 15 minutes after 1 hour irradiation. This is useful to understand the risk for the medical staff entering in the room after the treatment.

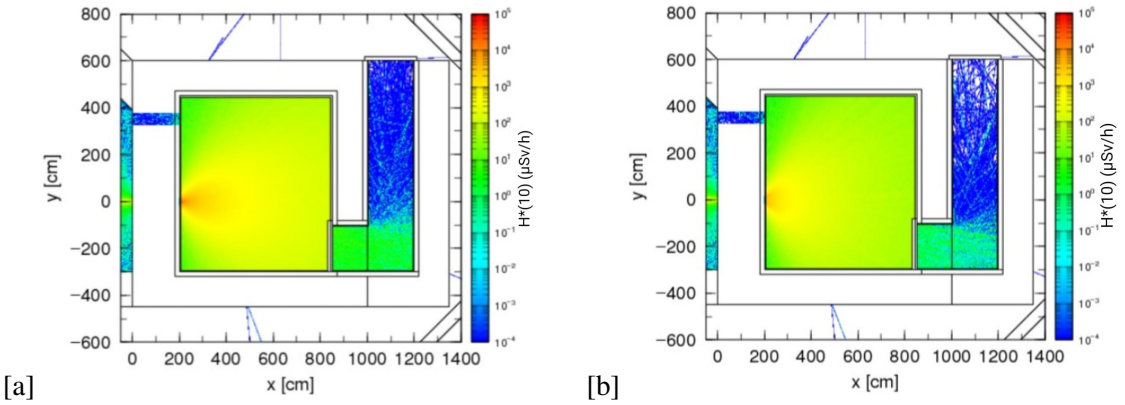

Figure 3.4: H*(10) in the room at 1s after 1h irradiation [a] without the shutter and [b] with the shutter.

Comparing Fig.3.4[a] and Fig.3.4[b] showing H*(10) due to BSA activation respectively without and with the shutter immediately after the end of the treatment, there is a clear reduction of the dose in front of the shutter. However this reduction is not comparable with the reduction achieved by moving the patient away from the irradiation position.

From a practical point of view, the use of an automatic shutter as the only strategy to protect the patient would not be wise, as a possible malfunctioning would expose patients to extra-dose. Thus redundancies would be necessary and the system would increase in complexity. This would also add extra burden for the authorization of the facility as a medical device. For these reasons, in addition to its small impact in dose reduction, the shutter can be considered as a secondary protection method while the patient is moved to a colder area. Figure 3.4 makes it clear that the chosen position is effectively the one where the dose due to BSA activation is lower in the room at the end of the treatment.

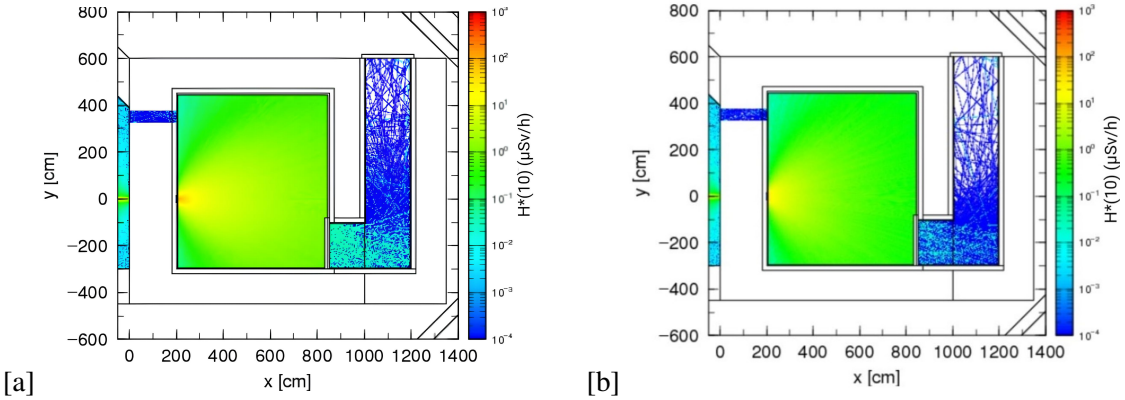

Figure 3.5: H*(10) in the room at 15m after 1h irradiation [a] without the shutter and [b] with the shutter.

Figure 3.5 shows the ambient dose in the room due to BSA activation without ([a]) and with

shutter ([b]) at 15 minutes after the irradiation. These maps have been represented in a different scale compared to Figure3.4, at 1 second. In fact, the goal was to enable an easy comparison of the shutter versus no-shutter situations at the same output times. After 1 second, in fact, the maximum ambient dose is two orders of magnitude higher with respect to 15 minutes, as also shown in Tables 3.10 and 3.11.

In the BNCT facility working in Xiamen, China, the patient protection after the treatment is based on the choice of moving the patient and use an automatic shutter which is positioned in front of the beam port as a further protection for the medical staff entering the room. In this way a possible malfunctioning of the shutter system does not cause an increase of the dose absorbed by the patient. The strategy proposed in this Chapter is thus adopted also in other BNCT centres currently treating patients.

In Chapter 4 these considerations will be extended to the robot for patient positioning and walls activation.

Chapter 4

Activation of the walls and of the room equipment

In Chapter 3 the necessity to move the patient away from the beam-port after the irradiation has been motivated. Patients are positioned in front of the beam-port according to the treatment planning using a robot. This device allows a precise positioning by reproducing the same configuration set-up in the preparation room. The immobilization devices and the software allow a precise positioning before the irradiation. The same robot is then used to move the patient in the chosen location of the room for the additional time needed. Automating the process allows reducing the time spent by the medical staff in the room. In this Chapter the influence on the ambient dose of the presence of the robot will be explored.

4.1 The robot

The mechanical structure of the robot occupies a large volume in the irradiation room. The choice of the materials for its construction is driven by the technological needs (movement and patient sustain) but also by sensitivity to neutron activation as low as possible. To simulate the structure I used information from the robotic arm used at NeuPex, the Neuboron Boron Neutron Capture Therapy AB-BNCT system, in Xiamen, China which is a KUKA R2700 model [31]. This robot (Fig. 4.1) has six degrees of freedom and it is partially covered with borated polyethylene that allows reducing the neutron activation. For mechanical reasons not all the robot surfaces can be lined, thus some metallic parts remain exposed to the neutron field in the room.

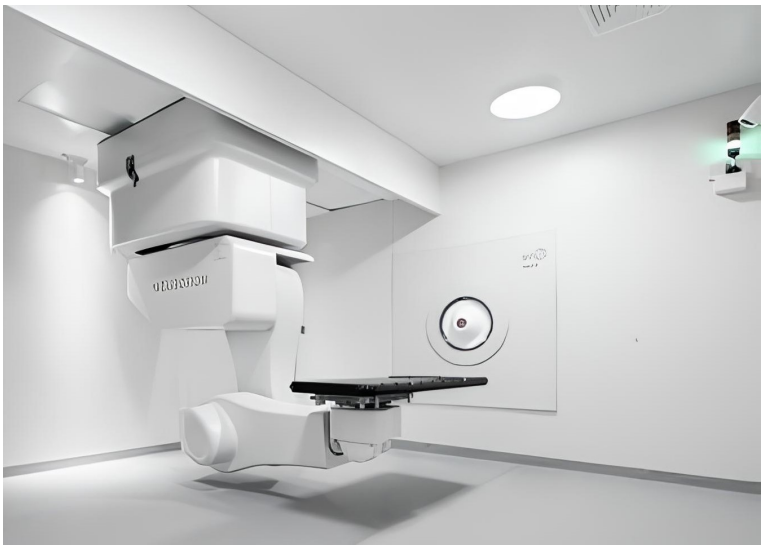

Figure 4.1: Robotic arms at Neupex AB-BNCT facility at Xiamen, China. Taken from [32].

The simulated robot (Figure 4.2) is a simplification of the one in Figure 4.1.

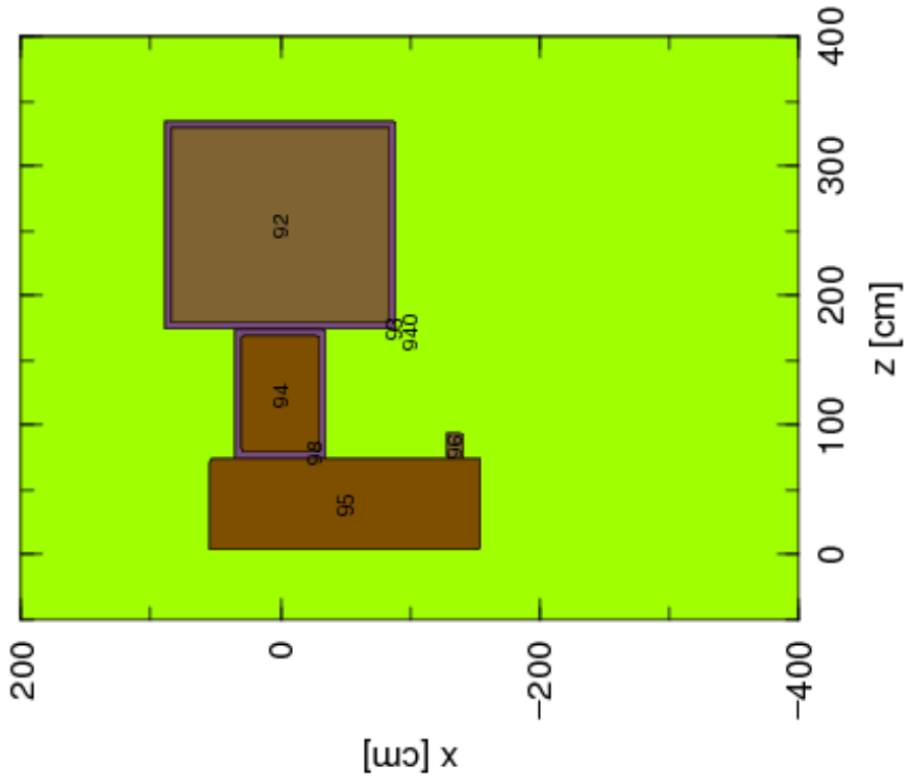

Figure 4.2: Simulated robot structure.

It is composed by:

- N°92: top part, attached to the ceiling, made by steel;
- N°93: top part polyethylene 5 cm cover to reduce the neutron activation;
- N° 94: top arm in aluminum;
- N° 98: top arm polyethylene 5 cm cover;
- N° 95: lower arm in aluminum;
- N° 96: couch support in steel.

The couch, made of carbon fiber, has been omitted from the simulation because it will not activate. The whole structure has been implemented and positioned in the room (Fig. 4.3) in a representative position for the treatment of the head and neck district irradiation.

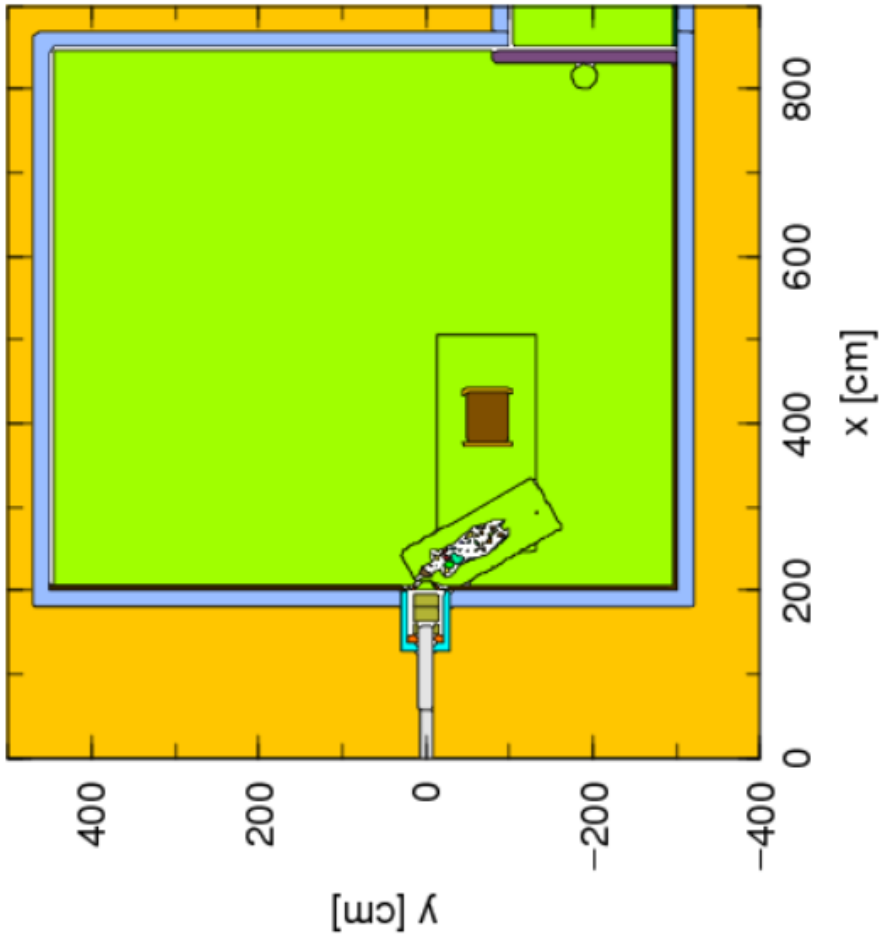

Figure 4.3: Robot position in the room.

It is interesting to evaluate both the activation of the robot itself and its impact on the walls activity

variation, if any. This structure in fact, being partially covered by borated polyethylene, which is a neutron absorber, can reduce the fraction of neutrons scattering in the room and reaching the walls, reducing also their activation.

With the robot positioned as described I have run 50 batches of 10^6 neutrons each with a `[T-Dchain]` tally in the regions of the robot, the walls, the floor and the ceiling. From the output files I have evaluated firstly the robot activation.

Table 4.1: Total number of γ-rays produced in the robot at 1 s and 15 m after 1h irradiation.

Region	1h+1s (s^{-1})	Rel. Err	1h+15m (s^{-1})	Rel. Err
92	$8.54{\cdot}10^6$	3.0%	$7{,}99{\cdot}10^6$	3.0%
94	$1.89{\cdot}10^5$	6.0%	$1.43{\cdot}10^5$	6.0%
95	$5.46{\cdot}10^7$	1.0%	$4.13{\cdot}10^7$	1.0%
96	$1.55{\cdot}10^7$	3.0%	$1.45{\cdot}10^7$	2.0%

Table 4.1 shows the number of γ-rays produced in the robot after one hour of irradiation. Regions 93 and 98, corresponding to the borated polyethylene, have been omitted because of their low gamma production (in the order of $10^{-15}s^{-1}$). The higher gamma production in regions 95 and 96 is due to the lack of polyethylene lining which, being a neutron absorber, reduces the radiation reaching the other regions. Compare the gamma production of regions 94 and 95 explains and quantifies the effect of the polyethylene cover. In fact, in these two regions made of the same material, the produced photons are about two orders of magnitude lower. It must be observed, however, that regions 95 and 96 could be characterized by a higher activation also because of their shorter distance from the beam.

Tables 4.2, 4.3, 4.4, 4.5, 4.6, 4.7, 4.8, 4.9 report, region by region, a list of the most activated nuclides.

Table 4.2: Region 92 activity at 1s after 1h irradiation. Uncertainty < 4%.

Isotope	Activity(Bq)	Relative Activity	Half-life(s)
^{56}Mn	$6.2978{\cdot}10^6$	97.77%	$9.284 \cdot 10^3$
^{55}Cr	$1.1665{\cdot}10^5$	1.81%	$2.098{\cdot}10^2$

Table 4.3: Region 92 activity at 15m after 1h irradiation. Uncertainty < 2.5%.

Isotope	Activity(Bq)	Relative Activity	Half-life(s)
^{56}Mn	$5.8890{\cdot}10^6$	99.46%	$9.284 \cdot 10^3$

Table 4.4: Region 94 activity at 1s after 1h irradiation. Uncertainty < 6.5%.

Isotope	Activity(Bq)	Relative Activity	Half-life(s)
^{38}Cl	$2.4424{\cdot}10^5$	98.63%	$2.234{\cdot}10^3$
^{35}S	$3.1681{\cdot}10^3$	1.28%	$7.561{\cdot}10^6$

Table 4.5: Region 94 activity at 15m after 1h irradiation. Uncertainty < 6.5%.

Isotope	Activity(Bq)	Relative Activity	Half-life(s)
^{38}Cl	$1.8478 \cdot 10^5$	98.19%	$2.234 \cdot 10^3$
^{35}S	$3.1678 \cdot 10^3$	1.68%	$7.561 \cdot 10^6$

Table 4.6: Region 95 activity at 1s after 1h irradiation. Uncertainty < 1%.

Isotope	Activity(Bq)	Relative Activity	Half-life(s)
^{38}Cl	$7.0559 \cdot 10^7$	99.64%	$2.234 \cdot 10^3$
^{35}S	$2.5367 \cdot 10^5$	0.36%	$7.561 \cdot 10^6$

Table 4.7: Region 95 activity at 15m after 1h irradiation. Uncertainty < 1%.

Isotope	Activity(Bq)	Relative Activity	Half-life(s)
^{38}Cl	$5.3887 \cdot 10^7$	99.52%	$2.234 \cdot 10^3$
^{35}S	$2.5365 \cdot 10^5$	0.47%	$7.561 \cdot 10^6$

Table 4.8: Region 96 activity at 1s after 1h irradiation. Uncertainty < 4%.

Isotope	Activity(Bq)	Relative Activity	Half-life(s)
^{56}Mn	$1.1439 \cdot 10^7$	98.00%	$9.284 \cdot 10^3$
^{55}Cr	$1.9621 \cdot 10^5$	1.68%	$2.098 \cdot 10^2$

Table 4.9: Region 96 activity at 1s after 1h irradiation. Uncertainty < 2.5%.

Isotope	Activity(Bq)	Relative Activity	Half-life(s)
^{56}Mn	$1.0696 \cdot 10^7$	99.57%	$9.284 \cdot 10^3$

The most important contribution to the activity in the robot comes from ^{38}Cl and ^{56}Mn. Their half-lives are, respectively, about 38 m and 2.5 h so, as observable in the tables, during the permanence of the patient in the room the main contribution to the dose will come from these nuclides.

To evaluate the ambient dose due to this activation I have generated the source from the `out-phits` file. Since the activated regions are large, unlike those composing the patient and the BSA, I have evaluated the neutron penetration inside the robot to reconstruct the source. Considering a large volume coated with a neutron absorber, in fact, there is the possibility that the neutrons distribute differently in depth. It is possible that increasing the depth the neutrons decrease thus also decreasing the induced activation. If this is case, a uniform distribution of the activation over the whole region, would no represent an accurate dosimetry in air, because the penetration of photons would be different. To assess this point, the neutron flux as a function of depth was simulated in the region with the goal of defining the source only in the volumes where activation is really produced.

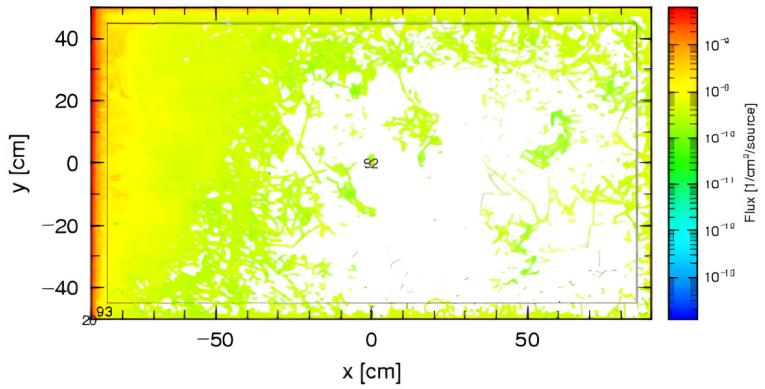

Figure 4.4: Neutron flux in the regions 92 and 93, xy view. The source is located at the top left of the images.

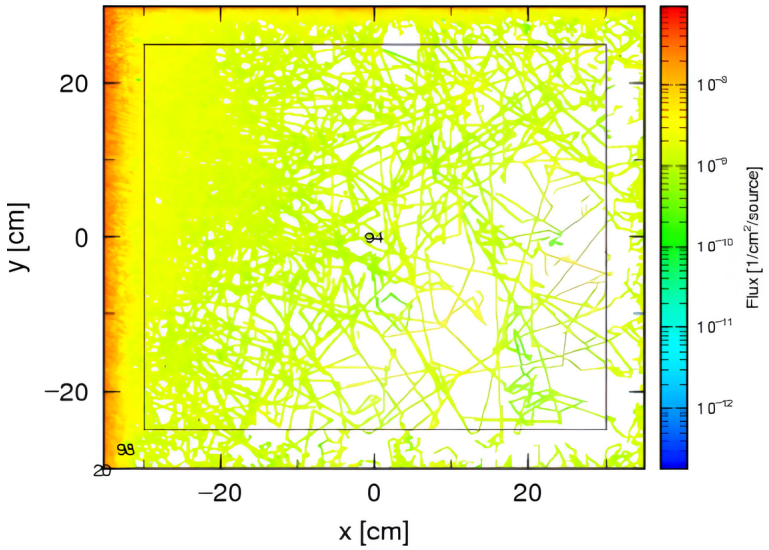

Figure 4.5: Neutron flux in the regions 94 and 98, xy view. Source is located at the top left of the images.

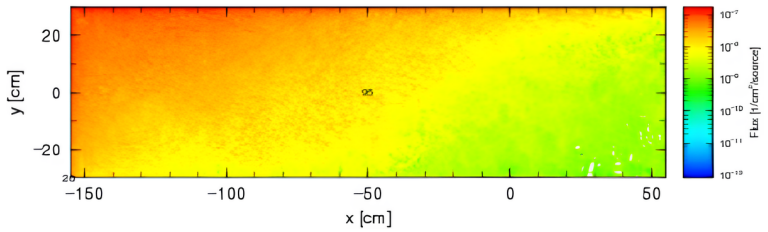

Figure 4.6: Neutron flux in region 95, xy view. Source is located at the top left of the images.

Figures 4.4 and 4.5 shows the xy view of, respectively, regions 92 and 94 each with its polyethylene layer which are clearly absorbing the most of the neutrons. It is clear that neutrons that pass through the cover are able, except for few cases, to penetrate for few tenth of centimeters along the x direction. In order to build the source in a realistic way and to maintain a conservative approach, I have decided to distribute the source activity from x=-80 cm to x=-50 cm for region 92 and from x=-30 cm to x= -20 cm in region 94. The absence of the polyethylene cover in region 95 (Fig.4.6) allows neutrons to penetrate deeper and reach the whole region. For this reason in this case I have considered the source as uniformly distributed in the entire volume.

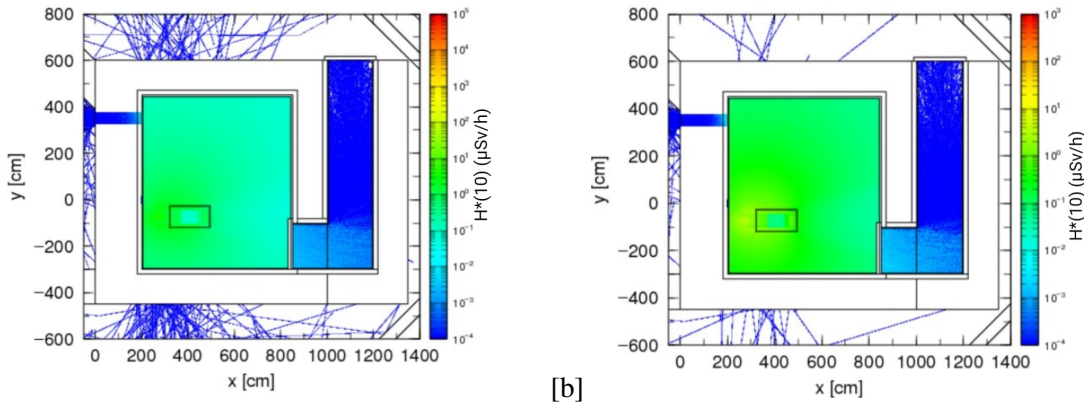

[a] [b]

Figure 4.7: H*(10) maps due to robot activation after 1h irradiation at [a] 1s and [b] 15 min. The scales are different to make it easier a further comparison between different activated zones at the same output times.

Figure 4.7 shows the H*(10) map due to robot activation. The ambient dose is realistically higher in the irradiated part of the robot as expected. The ambient dose is calculated only in air and not in the robot for this reason the value displayed in correspondence of the robot is due only to the air layer below the robot itself being thus lower than the rest of the room. Since the two scales are different, Table 4.10 lists the H*(10) maximum values at the output times for a better comparison. From this results, it is clear that the contribution of the robot to the dose is not relevant given the choice of this set of materials.

Table 4.10: H*(10) maximum values due to robot activation.

1h+1s (uSv/h)	Rel. err.	1h+15m (uSv/h)	Rel. err
7.24	1.0%	6.17	1.0%

4.2 Activation in the room walls

The robot covered in borated polyethylene might have influence on the walls activation. The wall, the composition of which has been already reported in Chapter 2, are simulated as shown in Figure 4.8.

As before, the numbers are associated to different regions:

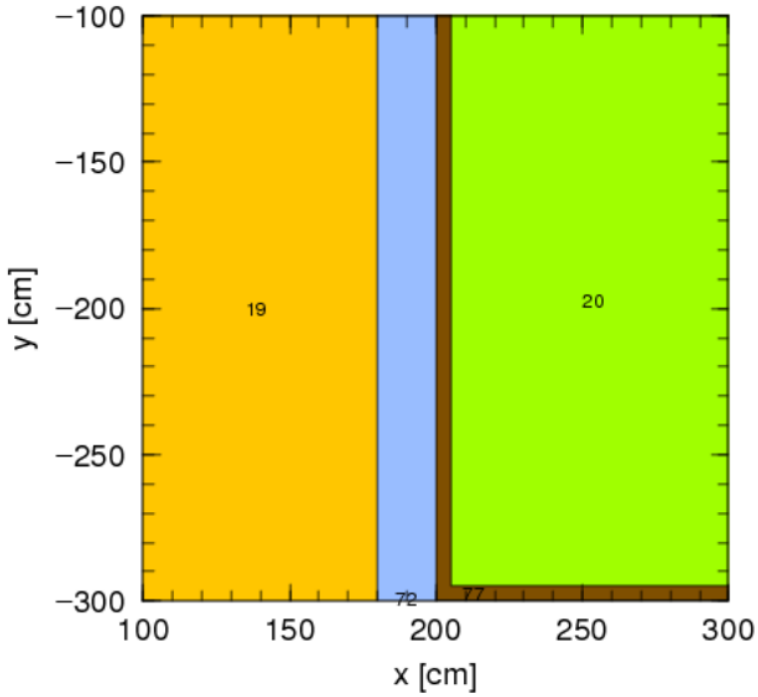

Figure 4.8: Particular of the simulation of walls structure.

- N° 19 is Portland concrete;
- N° 20 is the air inside the room;
- N° 72 is 20 cm thick baritic concrete;
- N° 77 is 5 cm thick borated polyethylene layer.

All the layers are repeated also for the ceiling in the same order, the floor instead is characterized by number 82 and it is made by Portland concrete only.

Table 4.11: Total number of γ-rays produced in the walls at 1 s and 15 m after 1h irradiation.

Region	1h+1s (s^{-1})	Rel. Err	1h+15m (s^{-1})	Rel. Err
19	$8.30{\cdot}10^{11}$	1.0%	$9.61{\cdot}10^{10}$	1.0%
72	$1.89{\cdot}10^{10}$	1.0%	$1.21{\cdot}10^{10}$	1.0%
82	$2.28{\cdot}10^{9}$	1.0%	$2.84{\cdot}10^{8}$	1.0%

Table 4.11 shows the total gamma production in the walls. Region N°77 is missing from the table because, due to its material composition, its activity is negligible with respect to the others. For each of these regions the most activated isotopes are reported.

Tables 4.12, 4.13, 4.14, 4.15,4.16, 4.17 list the activation produced in the walls at 1 second and 15 minutes after the end of 1-hour irradiation.

Table 4.12: Region 19 activity at 1s after 1h irradiation. Uncertainty < 0.1%.

Isotope	Activity(Bq)	Relative Activity	Half-life(s)
^{28}Al	$7.5625 \cdot 10^{11}$	89.83%	$1.345 \cdot 10^{2}$
^{24}Na	$4.4297 \cdot 10^{10}$	5.26%	$5.399 \cdot 10^{4}$
^{31}Si	$2.6824 \cdot 10^{10}$	3.19%	$9.438 \cdot 10^{3}$

Table 4.13: Region 19 activity at 15m after 1h irradiation. Uncertainty < 0.1%.

Isotope	Activity(Bq)	Relative Activity	Half-life(s)
^{24}Na	$4.3789 \cdot 10^{10}$	50.83%	$5.399 \cdot 10^{4}$
^{31}Si	$2.5110 \cdot 10^{10}$	29.15%	$9.438 \cdot 10^{3}$
^{28}Al	$7.3498 \cdot 10^{9}$	8.53%	$1.345 \cdot 10^{2}$

In tables 4.16 and 4.17, referring to the floor, the ^{40}K is between the three most activated isotopes while in tables 4.12 and 4.13, referring to lateral walls, it is not in the top three even if the material is the same. This is due to the fact that the concrete in the walls are covered by baritic concrete and borated polyethylene which shield the neutron interactions. This isotope has a relevant role particularly for the decommissioning phase due to its long half-life (about 10^9 years). The absence of ^{40}K in the list of the three most activated isotopes related to region 19 means that the shielding of thermal neutrons lowers its production. These study will be particularly useful for the decommissioning phase but the calculations will have to be repeated considering decades of operating period and alternating beam-on and beam-off cycles.

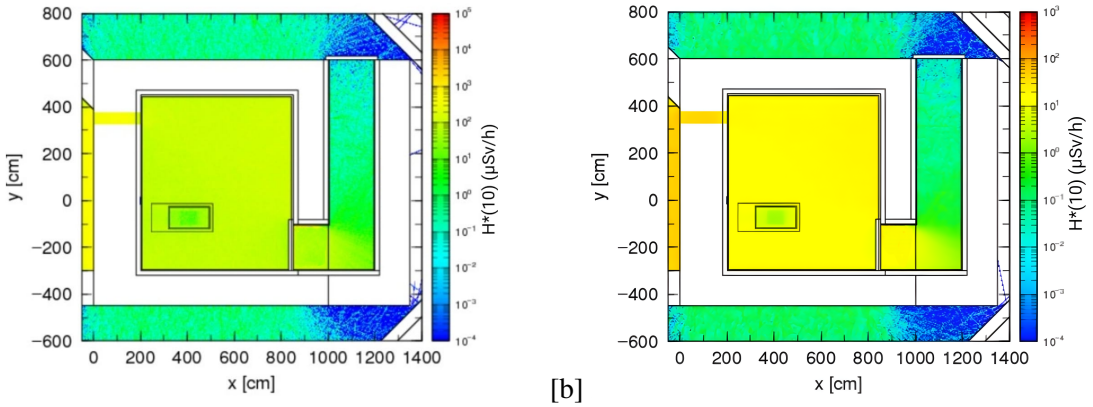

[a] [b]

Figure 4.9: H*(10) maps due to walls activation after 1h irradiation at [a] 1s and [b] 15 min. The scales are different to make it easier a further comparison between different activated zones at the same output times.

Figure 4.9 shows the H*(10) values inside the room due to the walls activation while Table 4.18 reports the maximum values of the ambient equivalent dose. It is also observable that there is an increase of the H*(10) behind the polyethylene door. It is not a real condition but it is an artifact due to the source definition.

Table 4.14: Region 72 activity at 1s after 1h irradiation. Uncertainty < 0.1%.

Isotope	Activity(Bq)	Relative Activity	Half-life(s)
^{139}Ba	$4.8192 \cdot 10^{10}$	86.11%	$4.384 \cdot 10^{3}$
^{28}Al	$4.8486 \cdot 10^{9}$	8.66%	$1.345 \cdot 10^{2}$
^{56}Mn	$1.5902 \cdot 10^{8}$	2.84%	$9.284 \cdot 10^{3}$

Table 4.15: Region 72 activity at 15m after 1h irradiation. Uncertainty < 0.1%.

Isotope	Activity(Bq)	Relative Activity	Half-life(s)
^{139}Ba	$4.2528 \cdot 10^{10}$	95.28%	$4.384 \cdot 10^{3}$
^{56}Mn	$1.4870 \cdot 10^{9}$	3.33%	$9.284 \cdot 10^{3}$
^{49}Sc	$1.4564 \cdot 10^{8}$	0.33%	$3.431 \cdot 10^{3}$

Table 4.18: H*(10) maximum values for walls activation: Condition 1 is at 1s after 1h irradiation, Condition 2 is at 15 m after 1h irradiation with robot and Condition 3 is as 2 but without the robot. Statistical uncertainty <7%.

Condition 1 (uSv/h)	Condition 2 (uSv/h)	Condition 3 (uSv/h)
$6.27 \cdot 10^{2}$	$4.87 \cdot 10^{1}$	$4.89 \cdot 10^{1}$

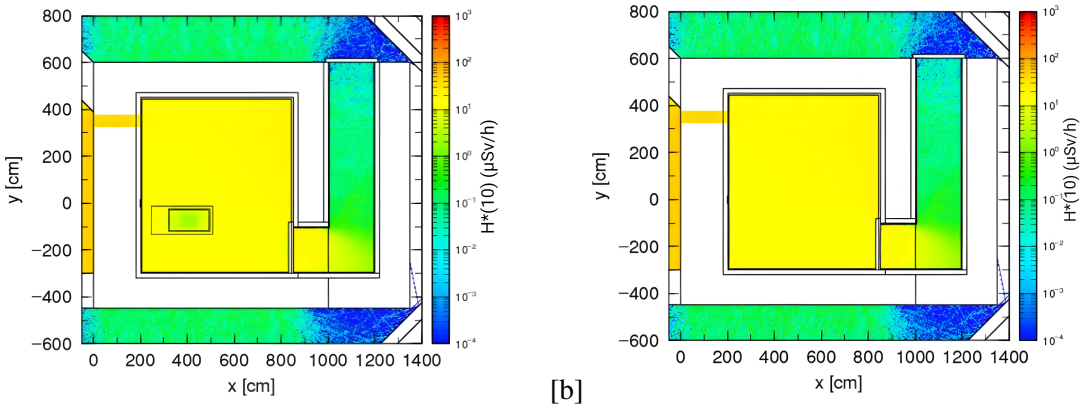

[a] [b]

Figure 4.10: H*(10) map of walls activation at 15m after 1h irradiation [a] with robot and [b] without it [personal communication, ongoing work for ANTHEM project].

To study the effect of the robot and its impact in modifying the dose due to wall activation, Figure 4.10 and Table 4.18 report a comparison of the situation with and without the robot. Figure 4.10 shows the H*(10) maps with and without the robot. Table 4.18 shows the maximum values of H*(10) due to walls activation. Comparing condition 2 and 3 it is clear that the robot presence does not influence the wall activity. The two values can in fact be considered equal within the statistical error.

Table 4.16: Region 82 activity at 1s after 1h irradiation. Uncertainty < 0.5%.

Isotope	Activity(Bq)	Relative Activity	Half-life(s)
^{28}Al	$2.0581 \cdot 10^{9}$	82.53%	$1.345 \cdot 10^{2}$
^{40}K	$1.9924 \cdot 10^{8}$	7.99%	$3.938 \cdot 10^{16}$
^{24}Na	$1.2105 \cdot 10^{8}$	4.85%	$5.399 \cdot 10^{4}$

Table 4.17: Region 82 activity at 15m after 1h irradiation. Uncertainty < 0.5%.

Isotope	Activity(Bq)	Relative Activity	Half-life(s)
^{40}K	$1.9924 \cdot 10^{8}$	45.61%	$3.938 \cdot 10^{16}$
^{24}Na	$1.1966 \cdot 10^{8}$	27.39%	$5.399 \cdot 10^{4}$
^{31}Si	$7.1847 \cdot 10^{7}$	16.45%	$9.438 \cdot 10^{3}$

4.3 Activation of the air in the irradiation room

Another component that must be considered in the activation analysis is air. Air, in fact, is composed by about 0.93% of argon (https://www.noaa.gov/jetstream/atmosphere), constituted by ^{40}Ar at 99.6%.
This isotope is stable but when it is irradiated with neutrons the reaction ^{40}Ar(n,γ)^{41}Ar occurs with a cross section of 0.66mb for thermal neutrons (https://www.nndc.bnl.gov/endf/). ^{41}Ar produced is a beta emitter and it is a problem because it is gaseous. The regulations fixes some limits for the release of ^{41}Ar outside the buildings, thus it is mandatory to predict the produced amount and to design a special system for the collection and exchange of air in ambient where high neutron intensities are present. This analysis was beyond the scope of my thesis, however it is important to stress that activation of air cannot be neglected in studies aimed at the authorization of neutron facilities. The main complexity of this calculation is the fact that the activity present in the room not only changes due to radioactive decay but also due to the air recycling. Thus, the evaluation of H*(10) requires the knowledge of technical aspects of the installation. The study of ^{41}Ar is also complex because the decree imposes the study of how the radioactive component will spread in the ambient outside the facility considering atmospheric conditions such as the wind. In the report that needs to be prepared for the authorization of the use of the ANTHEM research and clinical BNCT facility, the study of activation proposed in this thesis will be integrated with a dedicated study of ^{41}Ar production and discharge.

Chapter 5

Conclusions and future perspectives

The aim of this thesis was to evaluate the neutron activation of patients, treatment room and its equipment in order to calculate the ambient dosimetry to which medical and technical staff and other population will be exposed. The obtained results will be useful to obtain the approval for the AB-BNCT facility in Caserta. Presently, the preliminary report for the radiation protection has already been presented by the Radiation Protection Expert to the competent authorities. The next step will be the production of a more in-depth study, considering the detail of all the issues connected to radiation, comprising:

- Dosimetry outside the primary shielding
- Dosimetry in the rooms considering holes in the structure meant for cables and pipes
- **Activation of solid materials**
- Activation of liquid materials (like coolants, oils, greases)
- Activation of gases (air)
- **Activation and management of patients**
- management of possible radioactive sources meant for instruments calibration
- Discharge of irradiated waste and other materials used for research purposes
- The *sky-shine effect*, i.e., the reflection of radioactive elements present in the air released outside the building by atmospheric layers

This thesis contributes to the set-up of methods and software for the evaluation of two of these issues (in bold in the list above). The results are not to be considered complete yet, however, the construction of adequate computational instruments will make it straightforward to refine the calculations according to the requests of the Radiation Protection Expert in charge of the authorization. In this sense, the thesis offers a relevant contribution to the authorization process of the ANTHEM BNCT facility.

Regarding the patient, this thesis proposes, for the first time, a possible criterion to evaluate

the activation of the patient. A figure of merit has been chosen to compare the dosimetry due to activation of the BNCT patients against the case indicated in the decree which could be discharged without hospitalization. To this end, I have compared the ambient dose for the BNCT patient with the one due to 600 MBq of ^{131}I,representing the limit for the radiometabolic therapy indicated in the decree. The results listed in Table 2.43, show that the dose is two orders of magnitude lower in the BNCT cases with respect to the iodine case, already at 15 minutes after the irradiation. This means that the patient could be discharged few minutes after the end of the treatment. Considering that patients will remain under observation for a period of the order of one hour for medical purposes, I demonstrated that the activation is not an issue. This result holds for any of the three positions tested for irradiation (treatment in the districts of head and neck, thorax or lower limbs) and for the extremely conservative condition of 2-hours irradiation.

The results obtained in this thesis for the urine activation, combined with the those in [28], prove the necessity of a dedicated hot restroom. This finding has a direct impact on the design and management of the whole centre showing how much the radiation protection studies are pivotal at this stage of the projects.

In order to estimate the dose that the medical staff will absorb by working in the room, the ambient dose contributions due to the equipment and the walls were calculated. This will impact on the classification of the areas and of the staff from the radiation protection point of view and will help the Expert in charge to set the time limits of permanence in such ambient.

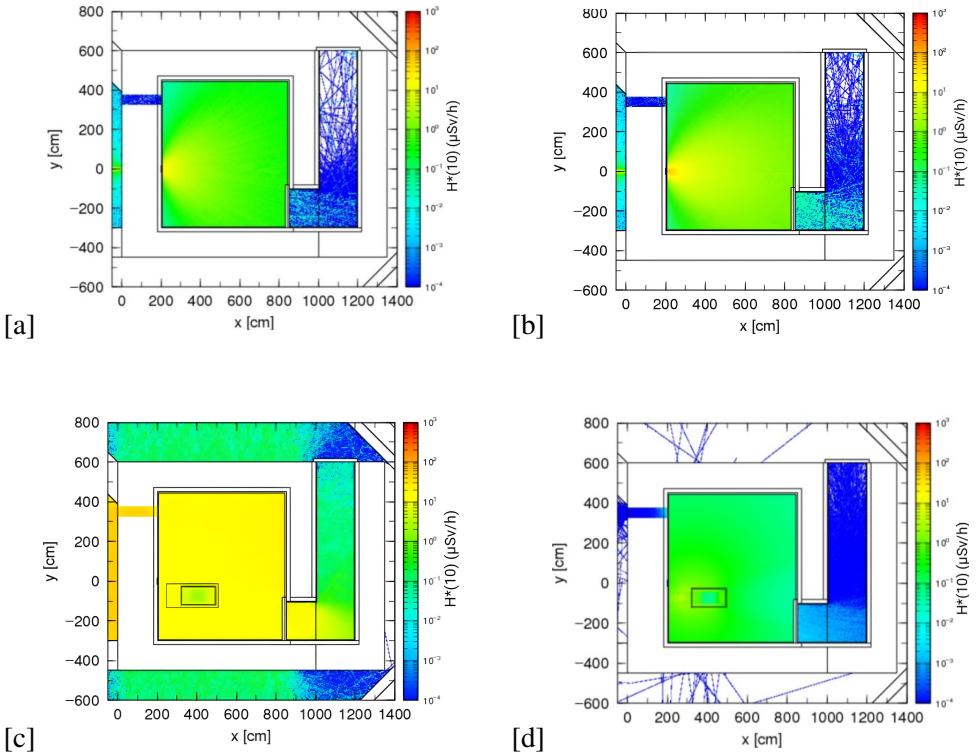

Figure 5.1: H*(10) at 15 minutes after 1h irradiation for: [a] BSA activation with shutter, [b] BSA activation without shutter, [c] walls activation and [d] robot activation.

Figure 5.1 shows a summary of the results obtained at 15 minutes after an irradiation of one hour for all the evaluated structures. It is clear that the main contribution to the ambient dose comes from the radioactivity produced in the walls, while the robot activation is almost negligible.

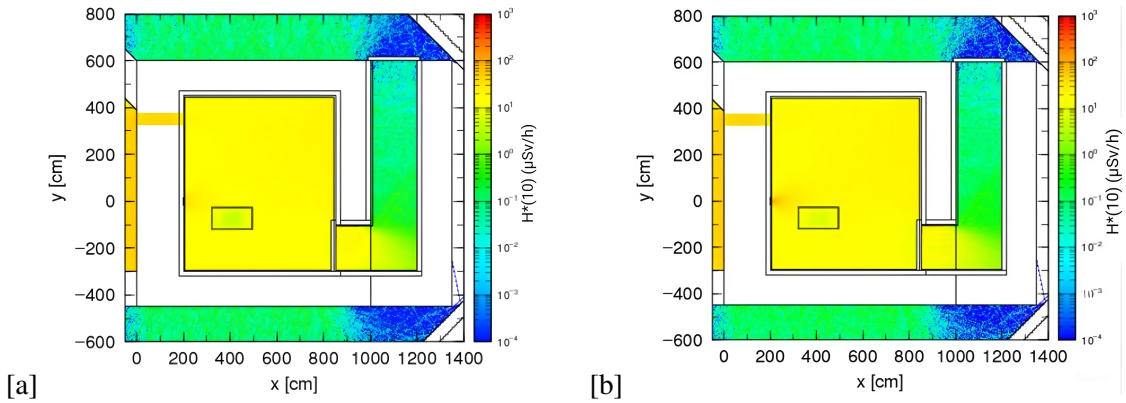

Figure 5.2: Summed results of the calculated ambient doses in the case with shutter [a] and without it [b].

Figures 5.2[a] and [b] refer to the sum of the calculated ambient doses due to all the contributions. These maps are useful to evaluate the risk of the staff entering in the treatment room and also the environmental dosimetric monitoring that may be necessary. Knowing the dose distribution gives useful indication about the classification of areas from the radiation protection point of view and on any access control to be set where threshold values are overcome.

In order to estimate the annual dose exposition for the medical personnel, a simplified calculation can be performed considering a worker who must stay in the irradiation room for 15 minutes, twice a day, 4 days a week for 40 weeks a year. These assumptions are justified especially at the beginning of the clinical activity, when we can expect a maximum of two treatments per day leaving many days a year for maintenance and technical work. This results in a time spent inside the room of approximately 80 hours per year. To be conservative, let us consider the maximum values of ambient dose due to the robot and the walls activation, the values between 30 cm and 40 cm for the patient thorax irradiation, which is the positing leading to the highest activation, and the mean value in the patient position for the BSA activation. The calculation uses the doses at 15 minutes after 1 hour irradiation time to obtain a realistic result of the dose at the time of the entrance in the room.

The result is about 90 $\mu Sv/h$ (with a statistical uncertainty lower than 5%) that, considering the previous approximations, means 7.2 mSv/year. The law limit of effective dose for workers professionally exposed to ionizing radiation is 20 mSv/year. Taking in account that the *ambient dose* is an operational quantity created to analyze the risk with a simpler approach it is possible to compare the results and the limits. However, it must be pointed out that the effective dose and the H*(10) do not refer to the same quantity. In addition it is necessary to underline that in this simplified calculation other components like the air activation are currently missing.

As anticipated above, the simulations performed in this thesis are a work-in-progress that will

be probably refreshed when all the components, like the BSA, will be in their definitive version. At that point, these computational instruments will be used also to understand the relevance of the induced activation in the context of the future decommissioning. Although the centre has not entered its construction phase, some strategies for the decommissioning must be already included in the radiation protection report. For this purpose, the calculations will be repeated alternating beam-on and off as expected in the clinical activity and considering many years of facility operation, thus reproducing the treatment and the maintenance cycles. For the calculations related to the decommissioning issues, trace element in the concrete and in the equipment will play an important role. These elements, in fact, being present in small amounts, do not produce a dose that can be a concern for daily work. For this reason, for the purposes of this thesis centred on the dosimetry in daily use, these traces have been neglected. However, it is known that concrete presents some traces that activate with neutron irradiation, for example the europium, which must be included in the long-time simulation. To be more precise, in the future work, we will measure the composition of samples of concrete at the TRIGA Mark II reactor of the LENA laboratory in Pavia, using the technique of neutron activation, as done before for the aluminium fluoride [33]. The real elemental composition will be then simulated and the long-term activation will be predicted. Some measures to reduce the materials activation in view of future decommissioning have already been implemented in the facility structure, for example in the three-layers structure of the walls.

A computational novelty introduced in this thesis is the use of ICRP computational phantoms, used for the first time in BNCT, demonstrating their compatibility with PHITS calculations. This opens new perspectives to their use also for the treatment planning and the optimization of the patient treatment.

This work has developed some computational tools and explored criteria for the radiation protection evaluation thus marking a step forward in the approval of the ANTHEM facility and in the beginning of BNCT treatments in Italy.

Bibliography

[1] Will Jin et al. "A Review of Boron Neutron Capture Therapy: Its History and Current Challenges". In: *International journal of particle therapy* 9 (June 2022), pp. 71–82. DOI: 10.14338/IJPT-22-00002.1.

[2] Leena Kankaanranta et al. "Boron neutron capture therapy in the treatment of locally recurred head-and-neck cancer: final analysis of a phase I/II trial". In: *International Journal of Radiation Oncology* Biology* Physics* 82.1 (2012), e67–e75.

[3] M. Sato et al. "Safety of Boron Neutron Capture Therapy with Borofalan(10B) and Its Efficacy on Recurrent Head and Neck Cancer: Real-World Outcomes from Nationwide Post-Marketing Surveillance". In: *Cancers* 16 (5 2024), p. 869.

[4] M. Sato et al. "Safety of Boron Neutron Capture Therapy with Borofalan(10B) and Its Efficacy on Recurrent Head and Neck Cancer: Real-World Outcomes from Nationwide Post-Marketing Surveillance". In: *Cancers* 16 (5 2024), p. 869.

[5] *Advances in Boron Neutron Capture Therapy*. TECDOC Series. Vienna: INTERNATIONAL ATOMIC ENERGY AGENCY, 2023.

[6] A.J. Kreiner et al. "Accelerator-based BNCT". In: *Applied Radiation and Isotopes* 88 (2014). 15th International Congress on Neutron Capture Therapy Impact of a new radiotherapy against cancer, pp. 185–189. ISSN: 0969-8043. DOI: https://doi.org/10.1016/j.apradiso.2013.11.064. URL: https://www.sciencedirect.com/science/article/pii/S0969804313005101.

[7] Naonori Hu et al. "Improvement in the neutron beam collimation for application in boron neutron capture therapy of the head and neck region". In: *Scientific Reports* 12.1 (2022), p. 13778.

[8] Ian Postuma et al. "A novel approach to design and evaluate BNCT neutron beams combining physical, radiobiological, and dosimetric figures of merit". In: *Biology* 10.3 (2021), p. 174.

[9] Jun Ma et al. "Loss odyssey in medical image segmentation". In: *Medical Image Analysis* 71 (2021), p. 102035. ISSN: 1361-8415. DOI: https://doi.org/10.1016/j.media.2021.102035.

[10] Chiara Magni et al. "Radiation protection aspects in the design of a Boron Neutron Capture Therapy irradiation room". In: *Radiation Physics and Chemistry* 218 (2024), p. 111621. ISSN: 0969-806X. DOI: https://doi.org/10.1016/j.radphyschem.2024.111621.

[11] A Pisent, E Fagotti, and P Colautti. "MUNES a compact neutron source for BNCT and radioactive wastes characterization". In: *Proc. Linear Accelerator Conf. LINAC*. 2014, pp. 261–263.

[12] Council of the European Union. *Council Directive 2013/59/Euratom of 5 December 2013 laying down basic safety standards for protection against the dangers arising from exposure to ionising radiation*. Official Journal of the European Union, L 13, 17.01.2014, p. 1-73. 2013. URL: https://eur-lex.europa.eu/legal-content/EN/TXT/?uri=CELEX:32013L0059.

[13] G Dietze et al. "ICRP Publication 123: Assessment of radiation exposure of astronauts in space". In: *Annals of the ICRP* 42.4 (2013), pp. 1–339.

[14] Günter Dietze. "Dosimetric Concepts and Calibration of Instruments". In: 2000. URL: https://api.semanticscholar.org/CorpusID:36618134.

[15] C Sneha. "ICRU report 95–Operational quantities for external radiation exposure". In: *Radiation Protection and Environment* 44.2 (2021), pp. 116–119.

[16] AA.VV. "ICRU Report 95: Operational Quantities for External Radiation Exposure". In: *Journal of the ICRU* 20.7 (2020).

[17] Daniele Introini. "Calcoli di radioprotezione e aspetti legislativi per la costruzione di centri clinici e di ricerca con fasci di neutroni - Msc Thesis - University of Pavia". In: (2024).

[18] J.W. Poston. "Dosimetry". In: *Encyclopedia of Physical Science and Technology (Third Edition)*. Ed. by Robert A. Meyers. Third Edition. New York: Academic Press, 2003, pp. 603–650. ISBN: 978-0-12-227410-7. DOI: https://doi.org/10.1016/B0-12-227410-5/00185-X. URL: https://www.sciencedirect.com/science/article/pii/B012227410500185X.

[19] Shoukat Khan et al. "Radioactive waste management in a hospital". In: *International journal of health sciences* 4.1 (2010), p. 39.

[20] Repubblica Italiana. *Decreto Legislativo 31 luglio 2020, n. 101*. https://www.normattiva.it/uri-res/N2Ls?urn:nir:stato:decreto.legislativo:2020-07-31;101. Attuazione della direttiva (UE) 2013/59/Euratom, che stabilisce norme fondamentali di sicurezza relative alla protezione contro i pericoli derivanti dall'esposizione alle radiazioni ionizzanti. July 2020.

[21] Robert L Harrison. "Introduction to monte carlo simulation". In: *AIP conference proceedings*. Vol. 1204. NIH Public Access. 2010, p. 17.

[22] Tatsuhiko Sato et al. "Features of Particle and Heavy Ion Transport code System (PHITS) version 3.02". In: *Journal of Nuclear Science and Technology* 55 (Jan. 2018), pp. 1–7. DOI: 10.1080/00223131.2017.1419890.

[23] Denise B. Pelowitz et al. *MCNP – A General Monte Carlo N-Particle Transport Code, Version 6.3*. LA-UR-23-10009. Los Alamos National Laboratory. Los Alamos, NM, 2023.

[24] Toshiyuki Sato et al. *PHITS: Particle and Heavy Ion Transport code System, Version 3.26*. Japan Atomic Energy Agency (JAEA). 2022. URL: https://phits.jaea.go.jp/.

[25] Chan Hyeong Kim et al. "ICRP publication 145: adult mesh-type reference computational phantoms". In: *Annals of the ICRP* 49.3 (2020), pp. 13–201.

[26] Bernd Grosswendt. *ICRP publication 110*. 2012.

[27] Stefano Agosteo et al. "Characterization of the energy distribution of neutrons generated by 5 MeV protons on a thick beryllium target at different emission angles". In: *Applied Radiation and Isotopes* 69.12 (2011), pp. 1664–1667.

[28] Chiara Magni et al. "Experimental and computational studies for an Accelerator-Based Boron Neutron Capture Therapy clinical facility: a multidisciplinary approach". In: (2022).

[29] HQ Woodard and DR White. “The composition of body tissues”. In: *The British journal of radiology* 59.708 (1986), pp. 1209–1218.

[30] A Selva et al. *Blistering Resistance of the MUNES Target Prototypes*. 2020.

[31] Jiang Chen et al. “Automated Robotic-Assisted Patient Positioning for Boron Neutron Capture Therapy: Integration with NeuMANTA Treatment Planning System and Dosimetric Impact Analysis”. In: (2024).

[32] *Neuboron Medical Group*. `https://en.neuboron.com/`. 2024.

[33] Chiara Magni. “Experimental and computational studies for an Accelerator-Based Boron Neutron Capture Therapy clinical facility: a multidisciplinary approach - PhD thesis - University of Pavia”. PhD thesis. 2022.